Universidad del País Vasco
Euskal Herriko Unibertsitatea
ZIENTZIA ETA TEKNOLOGIA FAKULTATEA
FACULTAD DE CIENCIA Y TECNOLOGÍA

Bachelor Final Project
Degree in Chemical Engineering

HZSM-5/SAPO-34 based catalysts for the transformation of dimethyl ether into olefins

Author:
Jon Ostolaza
Director:
Pedro Castaño

TABLE OF CONTENTS

1 INTRODUCTION

1.1 THE MARKET OF LIGHT OLEFINS

Olefins or alkenes are unsaturated chemical compounds with at least one double carbon-carbon bond with a general formula of $(CH_2)_n$ (Roberts and Caserio, 1977). Ethylene and propylene are the backbone of the petrochemical industry and they have gained interest during the last years as they are intermediates of many conversion, transformation and synthetic pathways (Olah, 2005). The annual demand of light olefins is a clear index of the evolution of the economic world, where the market demand reached to about 120 million ton per year for ethylene (Figure 1b) and 70 million ton per year for propylene (Figure 1c) in 2010 (Park et al., 2010). As it can be seen in Figure 1a, the vast majority of olefins (57%) is used in the polymeric world, specially to produce polyethylene (PE) and polyproplene (PP). Monomers and intermediates form the second largest group for olefin consumption (32%), comprising products such as ethylene oxide, monoethylene glycol, ethylene dichloride, ethylbenzene/styrene and propylene oxide (Chemsystems, 2007). Elastomers account for the majority of butadiene demand, styrene-butadiene rubber being the most important one (Rocha et al., 2007).

As previously stated, the major application of olefins is its use in the petrochemical industry, where PE and PP production accounts for 60 and 65% of the use of ethylene and propylene. The increasing substitution of other basic materials such as paper, steel and wood by PP will induce a further growth in the demand for PP, and hence, propylene. This can be seen in Figure 1b and 1c, where the expected annual growth rate of ethylene (4%) and propylene (5%) are shown. This difference in the growth rate is expected to continue for the next 10 years, meaning that propylene is gaining importance towards ethylene. Other common applications of ethylene are ethylene oxide and ethylbenzene, accounting for 10 and 8% of the total ethylene use, respectively. Another indicator of the increasing demand of propylene can be its application in a variety of products, as seen in Figure 1c.

The increasing demand of ethylene and propylene shown in Figure 1b and 1c, is driving new routes of production from natural gas and renewables (Al-Dughaither and De Lasa, 2009), together with the intensification of the already implemented industrial routes from fossil resources. For example, when considering natural gas, profits can be tripled by converting it into olefins rather than using it for combustion (Sardesai and Lee, 2006).

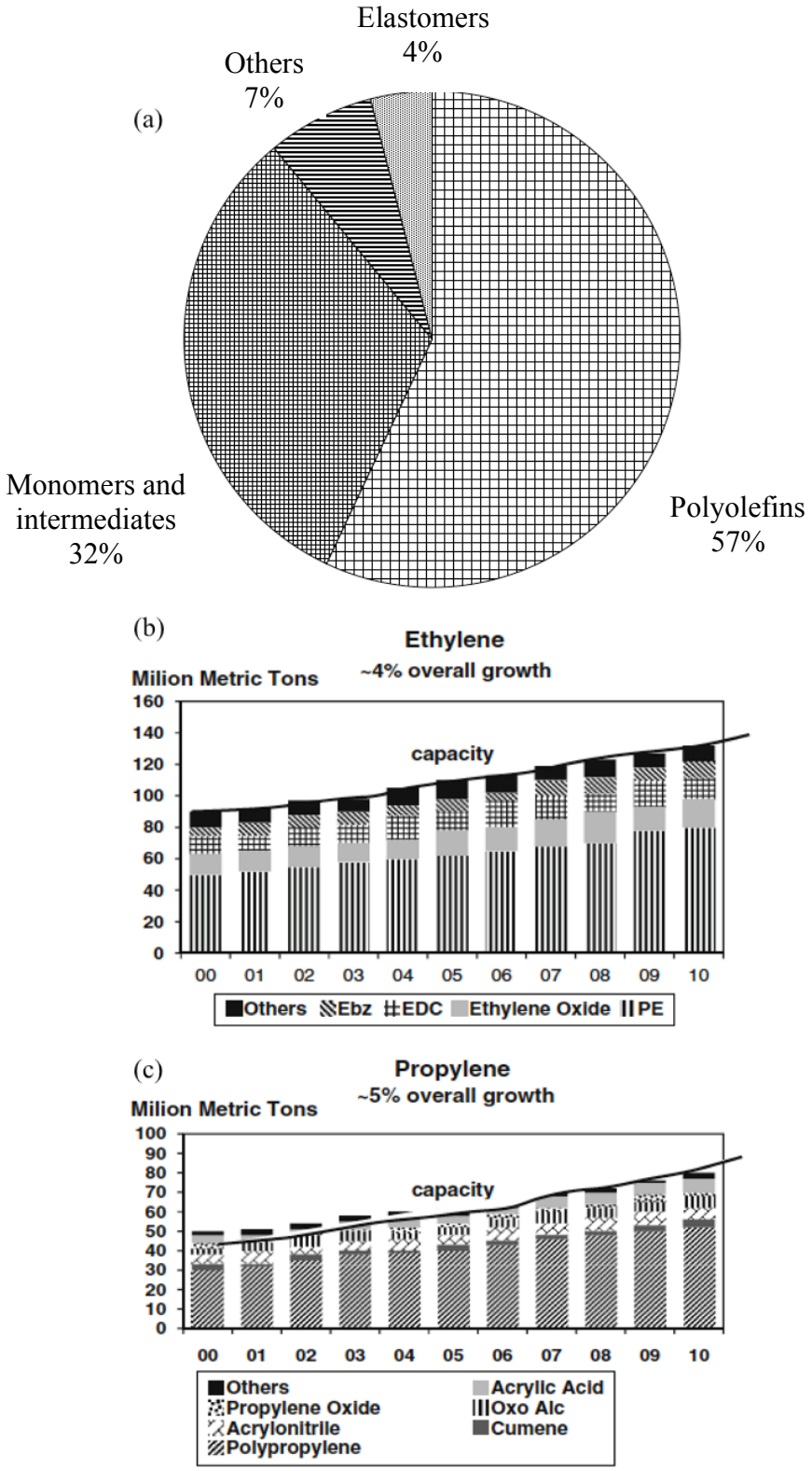

Figure 1. (a) Global olefin consumption, (b) global ethylene outlook and (c) global propylene outlook.

1.2 LIGHT OLEFIN PRODUCTION ROUTES

1.2.1 Steam cracking

Steam cracking is the main industrial source of propylene and ethylene, followed by fluid catalytic cracking (Figure 2a, showing only propylene, within "refinery"). This trend is changing towards other processes with higher importance like MTO or propane dehydrogenation (PDH) due to lower CO_2 emissions (Figure 2b). The global propylene capacity is increasing and expected to increase in the future (Figure 2), as its capacity is expected to increase approximately 100 million tons in only 25 years (from 72 million tons in 2005 to 165 million tons in 2030). This increase led to the development of new routes for propylene production. PDH and MTO processes have gained popularity (their contribution will increase 11 and 9% respectively until 2030), whereas the relative importance of both thermal and catalytic cracking will decrease by 15 and 7% by 2030. Nevertheless, in spite of this decrease, steam cracking and fluid catalytic cracking will continue to be the most used processes in propylene production in 2030 (47 and 26% of the global propylene capacity).

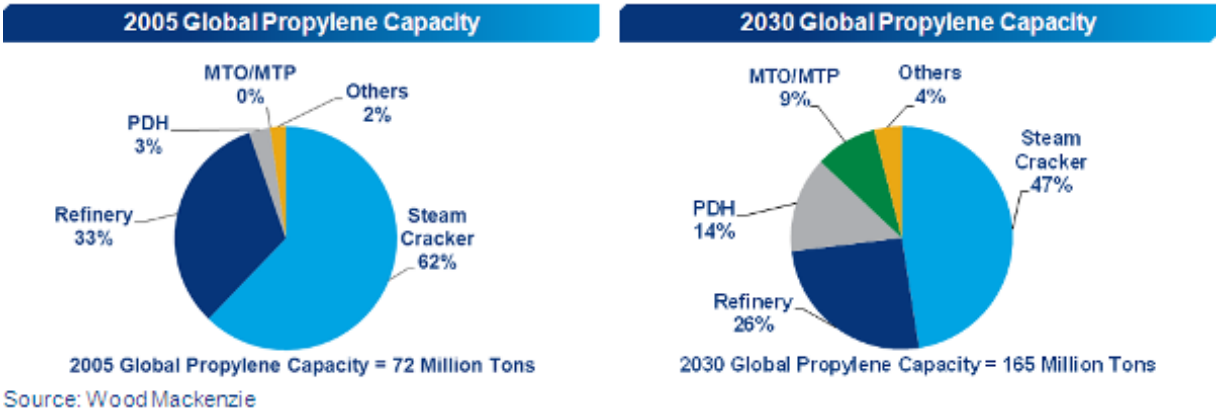

Figure 2. Global propylene capacity: (a) 2005; (b) 2030 (Wood Mackenzie).

Steam cracking is a thermal cracking conversion process, consisting on a series of pyrolysis steps where hydrocarbons are cracked into olefins and aromatics (recovered in what is known as pyrolysis gasoline or PyGas). Reactions take place in a furnace at 600–870 ºC and in presence of steam to provide heat and avoid coke formation. Selectivity towards olefins can be adjusted by controlling the temperature and the residence time of the reactants in the furnace (Al-Dughaither, 2014).

Steam cracking is usually carried out in a steam furnace made up of tube bundles where operating temperatures range from 815 to 870 ºC and the operating pressure is established to be 35 bar. In order to reduce coke deposition on the tubes and to enhance ethylene selectivity, steam is added as a solvent. Moreover, Chenier (2002) determined that the amount of steam increases with the density of the feedstock, varying from 0.3 kg steam/kg ethane (low density) to 0.9 kg steam/kg gas oil (high density). As it can be seen in Table 1, the selection of feedstock depends on the desired product, where the lighter the feedstock is, the lighter the produced compounds will be. For intance, a feedstock of ethane will give selectivity values for ethylene and propylene of 76 and 3% whereas a propane feedstock would decrease the

selectivity of ethylene to 42% and increase the one of propylene to 16%. Unfortunately, ethane cracking does not typically give enough propylene to be recovered. The amount of propylene recovered from propane, butane or even naphtha is less than half that of the ethylene yields efforts have been made in the last years to develop new feasible FCC technologies to increase even further the yield of propylene (Curtis et al., 2007).

Table 1. Selectivity of light olefins (wt%) from a cracking unit using various feedstocks. Adapted from Chenier (2002).

Product	Ethane	Propane	Naphta	Gas Oil
Ethylene	76	42	31	23
Propylene	3	16	16	14
Butene	2	5	9	9

Steam cracking consumes a considerable amount of energy and considerable coke formation takes place on the inner surface of the tube bundles, which drives a substantial downtime involved for cleaning the tubes and a drop in heat transfer efficiency. In order to avoid coke formation, wall temperatures are increased up to 1100 ºC, which on the other hand reduces the lifetime of the tubes (Mulla et al., 2002) and increases the formation of NO_x (Al-Dughaither, 2014).

1.2.2 Fluid catalytic cracking

Fluid catalytic cracking (FCC) is one of the essential conversion processes taking place at petroleum refineries. Normally, the process consists on converting vacuum gasoil into gasoline range hydrocarbons using a cracking catalyst. In this unit, significant amount of propylene is obtained as gaseous by-products (Park et al., 2010). As it can be seen in Figure 2b, FCC accounts for around 30% of the propylene production. The FCC unit consists on a fluidized bed where a gaseous flow moves the catalyst particles upward in the riser reactor. Due to the rapid deactivation of the catalyst, a regeneration unit is necessary. The superficial velocity in the riser is controlled for the entrainment of the catalyst along the gaseous hydrocarbon products.

As in thermal cracking, coke is also formed in FCC reactions. Nonetheless, in FCC coke deposits on the surface of the catalyst instead of in the tube as in steam cracking. Due to the fast deposition and, in consequence, the fast decrease in activity of the catalyst, it is vital to properly establish the operating conditions for catalyst regeneration and for coke combustion (Park et al., 2010). Usually, FCC units are built for the efficient utilization of energy where the heat released in the regenerator from coke combustion is conveyed to the catalyst to provide the necessary energy to vaporize the feed and for the endothermic reactions to take place (Chenier, 2002).

As formerly stated in section 1.1, ethylene and propylene market demand is considerably high and is expected to grow even further. However, there is a need for an alternative process for the production of propylene because the annual propylene/ethylene demand ratio is increasing

(Plotkin, 2005). In the past, FCC accounted for this shortfall but new technologies have been developed in the last decade to address this problem.

1.2.3 Methanol to olefins process

The methanol to hydrocarbons process over zeolites started out as a way to produce gasoline from coal. Nevertheless, when the demand for methyl tert-butyl ether decreased considerably due to environmental regulations, petrochemical companies started to investigate different and attainable uses for their already existing methanol plants. This is how the methanol to olefins (MTO) process started to gain popularity (AlWahabi, 2003). The interest on this process peaked in 1977 when Mobil's research group discovered the ZSM-5 (Zeolite Socony Mobil) zeolite catalyst. Besides ZSM-5, other catalysts like SAPO-34 or SAPO-18 have also been used in other companies like Norsk Hydro with promising results (Keil, 1999).

In the MTO process, methanol is first dehydrated to DME and the equilibrium mixture consisting of methanol, DME and water is then converted into light olefins. Then, olefins can react further to produce aromatics or paraffins via hydrogen transfer, alkylation or polycondensation (Al-Dughaither, 2014).

$$2CH_3OH \xrightarrow{-H_2O} CH_3OCH_3 \xrightarrow{-H_2O} \text{Light Olefins} \longrightarrow \text{Higher Olefins} \qquad (1)$$

1.2.3.1 MTP process of Lurgi

MTP process of Lurgi is a catalytic process where light olefins, specially propylene, are obtained from methanol. It is based on an efficient combination of the most suitable reactor system and a very selective and stable zeolite-based catalyst. A fixed bed reactor system was chosen to be used because of its many advantages over the fluidized bed reactor system, the main ones being the ease of scale-up and the significantly lower investment cost (Al-Dughaither, 2014).

The catalytic process is carried out using HZSM-5 (protonic form of ZSM-5 zeolite) as the catalyst, 1 bar pressure and temperatures ranging from 350 ºC to 500 ºC (Abramova, 2009). First, vaporized methanol is introduced into an adiabatic pre-reactor where it is partially converted into DME and water where the high-activity, high-selectivity catalyst used nearly achieves thermodynamic equilibrium. The resulting stream containing DME, methanol and water, is routed to the MTP reactor together with steam and recycled olefins. Conversion values of DME and methanol of 99% are achieved, propylene being the predominant hydrocarbon product. Process conditions in the five or six catalyst beds per reactor are controlled by feeding small streams of fresh feed between the beds, guaranteeing similar reaction conditions and maximum overall propylene yield.

The fixed bed reactor system consists of two reactors operating in parallel while the third one is in regeneration mode. Regeneration is necessary after 500-600 hours of cycle time because coke formed in side-reaction blocks the active catalyst centers. By using diluted air, regeneration takes place at mildest possible conditions, thus avoiding thermal stress on the catalyst (Koempel and Liebner, 2007).

1.2.4 Dimethyl ether to olefins process

The dimethyl ether to olefins (DTO) process could be considered as a modification of the MTO process, eliminating one step:

$$CH_3OCH_3 \xrightarrow{-H_2O} \text{Light Olefins} \longrightarrow \text{Higher Olefins} \quad (2)$$

This process has a series of advantages when comparing it to the MTO process:

1. *Higher hydrocarbon yield:* Complete conversion of methanol yields only one (CH_2) whereas two (CH_2) are obtained when DME reacts:

$$CH_3OH \longrightarrow [CH_2] + H_2O \quad (3)$$

$$CH_3OCH_3 \longrightarrow [CH_2 \cdot CH_2] + H_2O \quad (4)$$

   That is, for every mol of methanol converted, 14 g of hydrocarbons and 18 g of water are obtained, corresponding to a selectivity of 44 wt%. On the other hand, for every mol of DME reacted, 28 g of hydrocarbons and 18 g of water are obtained, accounting for a selectivity of 61 wt%. Thus, the yield of hydrocarbons is 38% higher using DME compared with methanol (Sardesai, 1997).

2. *Lower equipment costs:* The synthesis of DME is carried out in a single reactor whereas an additional dehydration reactor is usually needed for methanol production.

3. *Lower exothermicity:* The DTO reaction releases only 77.5% of the heat released on the MTO process because one exothermic dehydration step is eliminated (Al-Dughaither and De Lasa, 2009).

4. *Lower H_2/CO for DME synthesis:* A H_2/CO ratio of 2 is needed for methanol production (Equation (5)) while a ratio of H_2/CO of 1 is desired for DME conversion. By keeping the CO_2 concentration low, the effect of the WGS reaction is minimized, allowing to obtain DME with a H_2/CO ratio close to 1 (Chen et al., 2012).

$$2CO + 4H_2 \rightleftharpoons 2CH_3OH \rightleftharpoons CH_3OCH_3 + H_2O \quad (5)$$

5. *Reduced thermodynamic constraints:* In the MTO process, the water formed from Equation (5) promotes water gas shift reaction. On the other hand, when obtaining DME directly from syngas or using pure DME, the thermodynamic constraints for methanol become negligible, which leads to a notable reduction in operating pressures and yields of 90% for CO conversions.

Although the DTO process may seem an economically appealing option, its investigation is in its early stages, JGC/Mitsubishi being the only company to obtain high yield of propylene from DME (Markets and Markerts, n.d.).

1.2.5 Mechanism of the MTO/DTO process

During the last years, special attention has been given to the formation and degradation of the active state of the catalyst in the methanol to hydrocarbon (MTH) process. The mechanism and the catalytic site responsible for the formation of the first C–C bond and the build-up of hydrocarbon pool species has been extensively studied because the formation of the C–C bond is detrimental as it triggers the unwanted MTH reaction. The clear understanding of the reaction mechanism poses a huge challenge to the scientific world because it involves many elementary reactions ocurring in both competing and consecutive ways (Olsbye et al., 2015).

In the past, the traces of impurities on methanol or the catalyst was thought to be the responsible for the formation of the first C–C bond. However, Yiang et al. (2006) proved that impurities did not have a significant effect on the formation of the hydrocarpon pool (HCP) species. Since then, more than 20 mechanisms have been proposed in the literature, the most experimentally verified one being the "hydrocarbon pool" (HCP) mechanism (Gil-Coba et al., 2016).

1.2.5.1 Previously proposed direct mechanisms

1. *Oxonium ylide mechanism:* This mechanism relies on the formation of two important intermediates, *viz.* trimethyl oxonium (TMO) ion and dimethyl oxonium methyl ylide (DOMY) species. Transformation of TMO *via* Steven's rearrangement could produce methyl ethyl ether, thus providing the first C–C bond (Olah et al., 1984).

2. *Carbene mechanism:* Two different routes were proposed for the carbene mechanism: the α-elimination of water from methanol and the decomposition of surface methoxy species (SMS). The carbene species are then polimerized to form olefins or ethanol by concurrent sp^3 insertion into methanol or DME molecules (Olsbye et al., 2015).

3. *Methane-formaldehyde mechanism:* According to Nováková et al. (1987) methane was first formed before C_2^+ hydrocarbons at low methanol coverage in a mechanism consisting on two steps. First, reaction between methanol and SMS takes place to form methane and formaldehyde and to regenerate the acidic sites of the zeolite. Then, formation of the C–C bond by coupling the CH_3^- (obtained from previous deprotonation of methane to the zeolite conjugate base oxygen) with formaldehyde to form ethanol takes place.

Nevertheless, theoretical calculations have shown that the previously mentioned direct mechanisms cannot form a C–C bond from methanol or DME due to the high activation energies and unstable intermediates (Chowdhury et al., 2016).

1.2.5.2 "Hydrocarbon pool" mechanism

The "hydrocarbon pool" mechanism was stated by Dahl (1993) as a response to the controversy on the formation of the first C–C bond on the MTO process. This mechanism was stated when the existance of intermediates of polymethylbenzenium cations were found in SAPO-34 catalyst because it contains intersection boxes between channels that allow the stable location of the polimethylbenzenes.

Bjørgen et al. (2007) established the "dual cycle" mechanism to explain the formation of olefins over HZSM-5 zeolite, where the formation of polymethylbenzenes is more difficult comparing to SAPO-34 because of the lack of boxes that facilitate their stable location. In this regard, as the relative importance of each cycle depends on the shape selectivity of the catalyst, the methylation/cracking of olefins gains more importance than methylation/dealkylation of aromatics. The formation of olefins is therefore the consequence of the integration of both cycles. On the first cycle, ethylene is formed from polymethylbenzene by the methylation/dealkylation cycle of aromatics, whereas in the second cycle propylene and heavier olefins are formed through methylation/cracking of olefins. The integration of both cycles takes place because of the generation of aromatics by cyclation of the C_3^+ olefins formed in cycle two. The presence of these aromatics activates the first cycle, and olefins activate the second one.

1.3 DME AS A RAW MATERIAL

DME is the simplest ether with a chemical formula of CH_3OCH_3. DME is an invisible gas under standard temperature and pressure (STP) (1 bar and 25 ºC), having a larger density than air. On the other hand, when it is pressurized above 5 bar, DME becomes a liquid with a lower density than water (Arcoumanis et al., 2008). DME is a colorless, volatile, non-corrosive and non-toxic compound (Chen et al., 2016). During the last decade, the potential of DME as a clean and renewable energy source has been greatly investigated and this is closely related with its special features:

1. As DME does not form explosive peroxides, it can be stored and handled safely, unlike other ethers (Raoof et al., 2008).

2. As there are no C-C bonds on DME and 35 vol% is oxygen, the emissions of carbon monoxide and unburned hydrocarbons resulting from its combustion are less than those of natural gas.

3. Due to its high cetane number and low autoignition temperature, DME is considered as a clean alternative fuel for diesel engines. Moreover, when comparing it to the traditional diesel fuels, DME emitts less NO_x, forms fewer particulates and makes less engine noise (Hua et al., 2017). As the physical properties of DME and liquefied petrolium gas (LPG) are similar, DME can either replace or be blended with LPG, where mixtures up to 20 vol% of DME in LPG had no negative effect when using it for either heating or cooking (Fleisch et al., 2012).

4. As the vapor pressure of DME and LPG are very close, the current infrastructures for both storage and transportation could be used for DME, thus requiring no additional investment (Ladera et al., 2012).

Apart from its application as a substitute of LPG, DME is also used for the production of valuable chemicals like dimethyl sulfate, methyl acetate, methyl formate and light olefins through the DTO process (Arcoumanis et al., 2008). In addition to the previously mentioned

applications, DME is recommended as an environmentally friendly aerosol and green refrigerant due to its low toxicity, short average lifetime in the atmosphere (around 5 days) and zero ozone depletion potential (Lei et al., 2011).

1.3.1 Synthesis of DME

DME can be synthesized via a two-step process, which is the most conventional way, or directly from synthesis gas. In the indirect process, synthesis gas is first converted into methanol, and then, methanol dehydration takes place in another reactor, converting MeOH into DME (Azizi et al., 2014). The overall reaction mechanism corresponds to Equation **(**5).

The single step method, also known as syngas to dimethyl ether (STD) process, consists on obtaining DME directly from syngas in a single reactor using a bifunctional catalyst. These bifunctional catalysts are composed of a catalyst for methanol synthesis ($CuO–ZnO–Al_2O_3$) and another acidic catalyst for methanol dehydration (e.g., $\gamma–Al_2O_3$, zeolite, or ferrierite) (Zeng et al., 2013). The overall chemical reaction is displayed in Equation (6).

$$3CO+3H_2 \longrightarrow CH_3OCH_3+CO_2 \quad (6)$$

Each of the reactions above stated reaches maximum conversion when the H_2/CO ratio is close to the stoichiometrical value, i.e., 2 for Equation (5) and 1 for Equation (6). As the indirect process, the overall reaction of the indirect method is very exothermic and, therefore, it must be controlled for run-away avoidance. The main advantage of the direct process is that methanol synthesis and dehydration can be done simultaneously, easily overcoming the methanol synthesis equilibrium limitation by its in situ dehydration (Ereña et al., 2011).

1.4 DTO CATALYSTS

According to Ghavipour (2014) and Perez-Uriarte (2016b), catalysts such as SAPO-34 and HZSM-5 were favorable for the DTO reaction as well as the MTO reaction but with different efficiencies.

The ZSM-5 zeolite is an aluminosilicate zeolite where the precursor zeolite has a chemical formula of $Na_nAl_nSi_{96-n}O_{192}16{\cdot}H_2O$ where n is a number between 0 to 27, usually close to 3 (Froment et al., 1992). ZSM-5 belongs to the pentasil family of zeolites and has an inverted mordenite structure (MFI). A pentasil unit is made up of eight aromatic rings, each of them consisting of five sides. Their vertices contain either Al or Si and they are bonded with O. These pentasil units make pentasil chains by interconnecting with each other by oxygen bridges, arranging in a way that form corrugated sheets with ten-ring holes (Figure 3a). These sheets form a channel-based structure, where straight channels run parallel to the sheets and sinusoidal channels run perpendicular to the sheets as it can be seen in Figure 3b (Čejka and Bekkum, 2005).

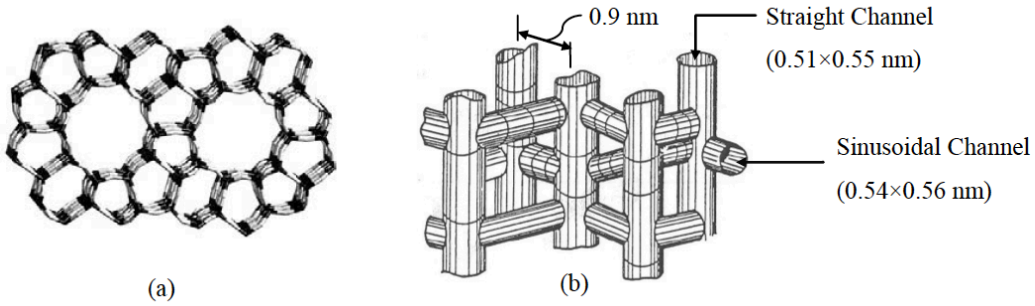

Figure 3. Structural diagram of ZSM-5: (a) face (100); (b) Micropore system.

Other zeolite structures can be formed by the replacement of Na^+ cations. For instance, they are substituted via ion exchange for H^+ cations to obtain its protonic form, HZSM-5 zeolite (Froment et al., 1992).

Silicoaluminophosphates (SAPOs) are another type of zeolite that are greatly used in the MTO process. The most used one is SAPO-34, where it is used in different industrial processes such as the Hydro/UOP process (Stöcker, 1999). The general chemical formula for SAPOs ranges from $0\text{-}0.3R\cdot(Si_xAl_yP_z)O_2$, where x, y and z have values that go from 0.01 to 0.98, 0.01 to 0.6 and 0.01 to 0.52, respectively, always complying $x + y + z = 1$. R represents the amine that is retained in the product and it is essential in the synthesis of SAPOs because amorphous materials are produced in its absence (Lok et al., 1984).

As it can be seen in Figure 4, the structure of SAPO-34 varies greatly from the one of ZSM-5. SAPO-34 has chabazite (CHA) type framework, with an average pore size of 0.43 nm. The structure of SAPO-34 is made up of six double rings arranged in layers to form a single cavity per unit cell. These double six-rings are arranged in parallel, thus having the same orientation. Figure 4a shows the interconnection of cages where each cage is connected to six others through octagonal openings of 0.44×0.31 nm. Figure 4b expands the view of one cage, having dimensions of 1×0.7 nm.

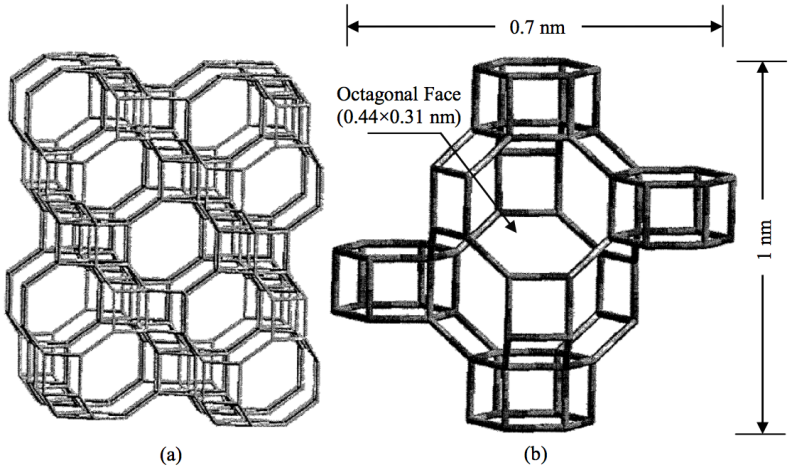

Figure 4. Structural diagram of SAPO-34: (a) Cage interconnections; (b) Cage dimensions.

In order to improve the characteristics of the catalyst, they are bound together with boehmite and alumina. This agglomeration improves the mechanical resistance and allows to work with a larger particle diameter, making it easier to use it in fixed bed reactors because there is no pressure drop and in fluidized bed reactors to avoid attrition problems (Michels et al., 2014).

Zeolite composite with binary structure is one of the most promising catalytic materials, because it can not only keep the nature of the individual zeolite but also give rise to new distinctive properties (Duan et al., 2011). In this regard, different HZSM-5/SAPO-34 composites have been studied and compared to independent HZSM-5 and SAPO-34. According to Duan et al., 2013, the HZSM-5/SAPO-34 composite obtained from both hydrothermal synthesis and physical blending showed higher propylene yield in the transformation of oxygenated compounds, the maximum being 34.5%. Therefore, it is deduced that synergetic effect of SAPO-34 and HZSM-5 occurred in HZSM-5/SAPO-34 composite catalyst. In this work, the kinetic performance of HZSM-5 and SAPO-34 as well as a composite catalyst that was obtained by physical blending from the previous two has been studied using DME as the feed at different space times and temperatures. In order to analyze the results, the selectivity and yield of olefins and the conversion of DME has been taken into account.

2 OBJECTIVES

The main goal of this work is to evaluate the behavior of the different acid catalysts on the transformation of DME to olefins, using both commercial catalysts and its modifications on the form of composites. In order to do so, catalysts with two different structures have been tested: HZSM-5 zeolite and SAPO-34 as well as the combination of the previous catalysts in the form of a composite in order to find possible synergic effects that can improve the kinetic performance of the catalyst. The milestones proposed for reaching the main goal are:

- Prepare different acid catalysts agglomerated in a γ-Al_2O_3 matrix to make their use at industrial level and the comparison between composites and individual catalysts possible.
- Characterize the physicochemical properties of each catalyst to evaluate the effect of the binder and the active phases on the surface of the catalyst.
- Evaluate the effect of temperature and space time on the different reaction indexes (conversion, yields and selectivities) of each one of the reaction products for each catalyst.
- Study the evolution of each one of these indexes with the time on stream and the deactivation of each one of the prepared catalysts.

3 MATERIALS AND METHODS

3.1 CATALYST PREPARATION

18.5 cm^3 of colloidal dispersion of α-alumina (Alfa Aesar, 20 wt% Al_2O_3) were poured in a vessel with constant stirring speed and 9.09 g of boehmite (Sasol Germany, 70% Al_2O_3) were added little by little. In the meantime, deionized water was being poured every now and then in order to keep the solution liquid enough to ensure homogeneity. Finally, 10 g of the active phase were added to the solution. When synthesizing the catalyst containing either pure HZSM-5 (Zeolyst International, SiO_2/Al_2O_3 molar ratio 15) or SAPO-34 (Johnson Matthey Catalyst) as the active phase, 10 g of these materials were used, whereas in the case of the composite, the corresponding amount of HZSM-5 and SAPO-34 was used. Due to the hydrophylicity of HZSM-5, the samples were dried before weighing. After three hours of mixing, the catalyst particles were obtained by wet extrusion. The extrudates were dried at room temperature for 12 hours, and after that, they were sieved to a particle diameter between 0.125 and 0.300 mm, which is the desired size to be used in a fixed bed reactor with low pressure drop.

Calcination of the catalyst was carried out in a muffle furnace (Termicon P, Heraeus). The particles were first heated at a constant rate of 5 ºC min^{-1} for 110 min and afterwards they were calcined at 575 ºC for two hours. In the end, the samples were left in the furnace for another two hours while cooling. The catalysts were synthesized to contain 50% of active phase, 30% boehmite and 20% alumina embedded in γ-Al_2O_3 matrix, which is the product of boehmite calcination. Moreover, the γ-Al_2O_3 matrix provides the catalyst with a hierarchical mesoporous structure.

3.2 CATALYST CHARACTERIZATION

For the better understanding of the different catalysts, various characterization equipments have been used to analyze the physical, structural and acidic properties of the catalysts synthesized.

3.2.1 Adsorption-desorption of N_2

The physical adsorption of gases or physisorption is a broadly used technique to determine the specific surface area of a catalyst or any porous material. In this case, the BET surface area (S_{BET}), the mesopore surface area (S_{mes}), the micropore volume ($V_{micropore}$) and the mesopore volume ($V_{mesopore}$) of the catalysts were determined from N_2 adsorption-desorption at -196 ºC in a Micromeritics ASAP 2000. The surface area was determined using Brunauer-Emmett-Teller (BET) equation, the mesopore surface area and the micropore volume was calculated from *t*-method based on the Harkins-Jura equation and the mesopore volume was computed as the difference between the total pore volume and micropore volume.

To start off, the samples were degased for 8 hours at 150 ºC to remove the impurities. Then, the samples were weighed and the mass loss is written down. The physisorption unit measures

the volume of gas adsorbed at relative pressures that vary from 0.01 to 1 at -196 ºC. In order to make the adsorption-desorption isotherms, the unit adds nitrogen and waits for stationarity to be achieved. Once stationary state has been achieved, the unit notes down the value and increases the added amount of nitrogen, thus, increasing the relative pressure in the case of adsorption and decreases the added amount of nitrogen, decreasing the relative pressure for desorption.

3.2.2 X-Ray Diffraction

X-Ray Diffraction (XRD) is the main technique used to analyze the internal structure of crystalline solids. The procedure consists on bombarding the sample with electrons at different angles (θ) and recording the intensity of the reflected X-ray. When the geometry of the incident X-ray hitting the sample satisfies Bragg's Law, a peak in intensity occurs. This law relates the wavelength of electromagnetic radiation (λ) to the diffraction angle (θ) and the lattice spacing (d). The final graph, also called diffractogram, consists on a series of arbitrary units along different angles. The diffraction peaks are then converted to d-spacings, allowing the identification of the material because each compound has a set of unique d-spacings. For X-ray powder diffraction, the values for 2θ go from 3.5º to 60º, with a 0.0262º gap between each measurement.

$$n\lambda = 2d \sin\theta \tag{7}$$

The analysis were carried out in Servicios General de Investigacion (SGIker) in Leioa using a PANalytical Xpert PRO diffratometer equipped with a copper tube as the target material ($\lambda CuK\alpha_1$= 0.15406 nm, $\lambda CuK\alpha_2$ = 0.15443 nm and $\lambda CuK\alpha_{avg}$ = 0.15418 nm) and Bragg-Brentano geometry.

3.2.3 Adsorption-desorption of NH_3

The total acidity and acid strength distribution of the of the catalyst was studied by adsorption-desorption of NH_3 at 150 ºC, using a Setaram DSC-111 calorimeter. Then temperature programed desorption (TPD) was performed, recording the ammonia signal (m/z = 15) in a mass spectrometer (OmniStar, Balzers Instrument) and rising temperature at 5 ºC min^{-1} up to 550 ºC.

The study was done in a Setaram DSC 111 calorimeter connected to a Harvard injection pump, where the heat flux and the variation of the adsorbed mass is measured at the same time. The equipment is also coupled on-line to a Thermostar mass spectrometer from Balzers Instruments. The total quantity of NH_3 retained chemically corresponds to the total acidity per unit mass of the sample.

The experimental procedure consists on five different stages. First, the sample is swept with He at a flow rate of 60 ml min^{-1} at 550 ºC for 30 min to get rid of the impurities. Then, stabilization of the process at 150 ºC occurs at a He flow rate of 20 ml min^{-1}. After that, saturation of the sample at 150 ºC takes place by the continuous inyection of NH_3 (50 µl min^{-1}) through a syringe. When saturation has been reached, the sample is then swept again with He at a flow rate of 20 ml min^{-1} in order to remove the physisorbed adsorbate. The

base is desorbed by heating the sample until 550 ºC at a heating velocity of 5 ºC min^{-1} and registering the intensity of the NH_3 signal in a mass spectromter. The reason for the previously stated heating velocity corresponds to the capacity to distinguish the nature of the acid sites. The weak acid sites are desorbed at low temperatures whereas the strong acid sites are desorbed at high temperatures. The total amount of NH_3 retained chemically corresponds to the total acidity or the number of acid sites in the sample ($mmol_{NH_3}\ g_{cat}^{-1}$).

3.2.4 Thermogravimetric-Temperature Programmed Oxidation (TG-TPO)

The amount of coke that is deposited on the catalyst is calculated and characterized through temperature programmed oxidation (TPO), where air acts as the oxidizing agent. The experiment was carried out using a TA Instrument TGA Q6000 thermobalance, which is connected to a Balzers Instruments Thermostar mass spectrometer.

The experimental procedure consists on 2 main different stages. On the first one, the sample is heated to the reaction temperature with N_2 at a ramp of 10 ºC min^{-1} and is kept for approximately 10 min. Later, the samples are cooled down to 50 ºC with N_2 and after that a second heating phase takes place at a ramp of 5 ºC min^{-1} until it reaches 550 ºC and the sample is then oxidized for 1 hour. Nevertheless, unlike in the first heating cycle, air is used in the second one instead of N_2. In the first stage the carbonaceous species trapped or adsorbed on the catalyst surface are desorbed, while in the second one the coke is burnt and its total amount is obtained.

3.3 REACTION SYSTEM

3.3.1 Reaction equipment

The reactions have been carried out in an automatic reaction equipment (PID Eng. & Tech. Microactivity Reference), whose diagram can be seen in Figure 5. The equipment is made up of a fixed bed reactor and a micro gas chromatography (Agilent 3000A) for the analysis of the reaction products. The control system of the variables is done with a software called Process@.

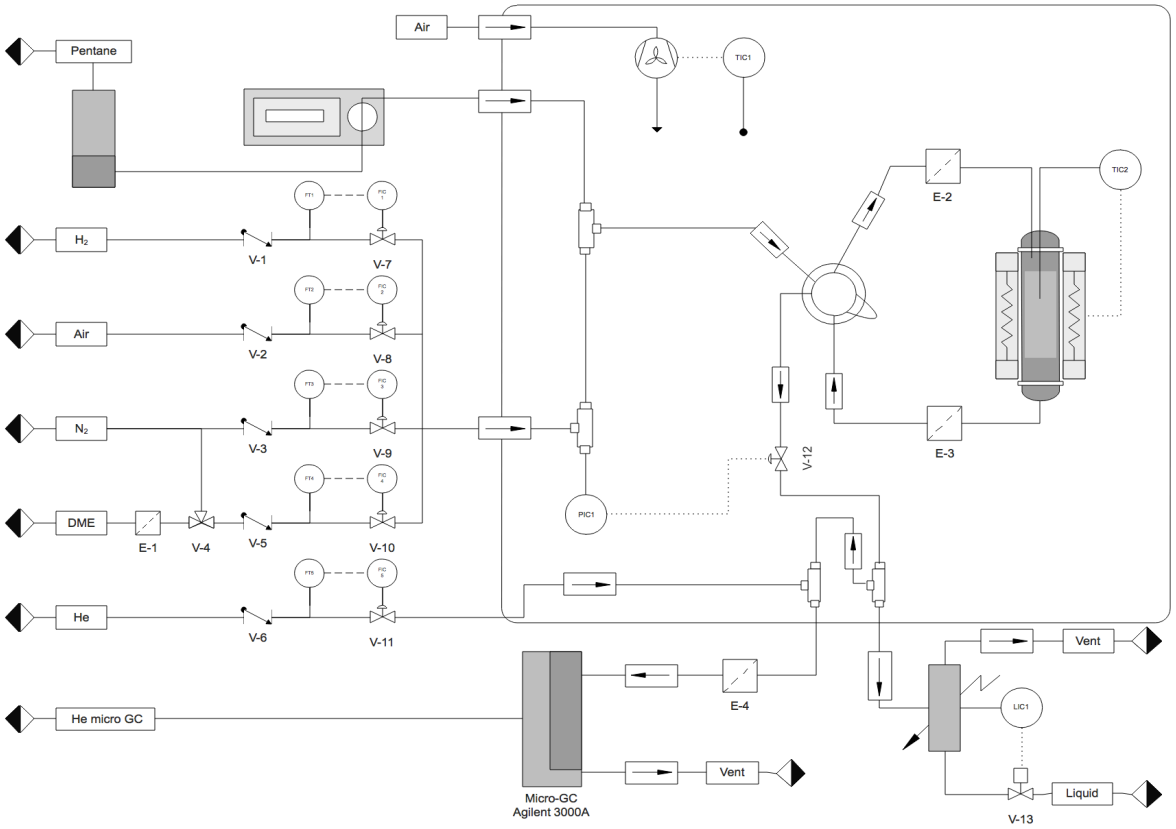

Figure 5. Diagram of the reaction equipment.

The gases are fed to the system through a series of mass flow controllers (Bronkhorst High-Tech B.V. Series) that are complemented with shut-off and check valves in order to maintain gas flows in one direction and to avoid backflow. These mass flow controllers are independent to the changes in temperature and pressure and they have been provided with a unit to measure and control the flows from 10 to 100 ml_{STP} min^{-1}.

The gases fed to the reaction system are the following:

- Inert gases: N_2 and He to sweep gases to the chromatography unit.
- Reaction gas: DME
- Oxidizing agent: Air

In cases where pentane was necessary, the addition of the liquid was done by a high pressure syringe pump (Harvard Apparatus PHD Ultra) and a 8 ml high pressure stainless steel syringe which allows the user to operate at flow rates from 29.5 µl min^{-1} up to 31.2 ml min^{-1}.

Due to several problems regarding the DME feed and its corresponding mass flow meter, a filter has been introduced before the mass flow meter. If the removal of impurities does not occur, these pollutants get stuck in the mass flow meter, leading it to its breakage. Moreover, a three-way valve has been used to clean the mass flow meter with N_2 after DME has gone through.

The gaseous and liquid feeds are then mixed together in a hot box where they are homogenized and preheated to 140 ºC to avoid condensation. Later the feed reaches a 6-port pneumatic valve allowing the user to send the reactants to the reactor or to the gas exit and to the analysis system in bypass mode, which is vital to know the composition of the feedstock.

The reactor (Autoclave Engineers) is made of 316 stainless steel with an internal diameter of 9.1 mm. The reactor has a length of 305 mm, where the effective length is of 100 mm. The reactor is capable of withstanding temperatures up to 800 ºC, pressures up to 100 bar and a catalytic mass of 5 g. The reactor is located in the interior of a stainless steel cylindric vault heated by a ceramic-covered electrical resistence.

The catalytic bed is made up of the catalyst and carborundum (VWR Chemicals) with a particle diameter of 500 mm. The particle diameter of the inert material has been chosen to be larger than the one of the catalyst to facilitate the recovery of the catalyst using a molecular sieve after reaction has taken place. Moreover, a layer of quartz wool (Panreac Quimica) has been introduced on top and on the bottom of the catalytic bed, to achieve the desired height and to make sure the gas flow follows the right route, the reactants being fed from the top of the reactor and the products leaving it from the bottom. Filters have been used before and after the reactor in order to avoid breakage of the valve system from catalytic particles.

The temperature of the reactor is measured with type K thermocouples and is controlled using digital temperature controllers (TOHO TTM-005 Series). There are two thermocouples in the reactor: the first one goes through the catalytic bed and the second one is on the reactor chamber wall. Two additional thermocouples are located in the reaction system, where the first one measures the temperature of the oven and the second one the temperature of the feed line that goes to the micro-GC.

Pressure is measured at the exit of the reactor using a pressure gauge of type Sensor-Technik-Wiedemann its range going from 100 mbar to 100 bar. On the other hand, the pressure controller (TOHO TTM-005) acts upon a needle valve depending on the flow passing the reactor.

Finally, 1 cm^3 of the reaction products are diluted in He with a flow rate of 40 ml min^{-1} and is send to the micro-chromatography unit every 8 min for its analysis. The other part of the reaction products goes through a Peltier cell, at 0 ºC, where the heaviest compounds are condensed and the non-condensable gases are vented to the atmosphere. The reaction system also has a level sensor and a level indicator controller that acts upon a needle valve for the extraction of the condensed liquids.

3.3.2 Control system

As previously stated, the operation variables are controlled through a control software called Process@. This software allows the user to create different sessions corresponding to the different stages of the process and to execute them in line. In this case, 12 sessions have been described.

3.3.2.1 Sessions for the pretreatment of the catalyst

Session 1: Communication is established between the reactor and the control software and the process is started.

Session 2: N_2 and He are fed to the reaction system and to the Micro-GC at 20 and 40 ml min^{-1} respectively.

Session 3: The reactor is heated to 300 ºC while the feed is changed to bypass mode. This session lasts 2000 seconds.

Session 4: The feed valve of N_2 is closed and the one relative to air is opened, feeding air at 30 ml min^{-1} for 15 min.

Session 5: The reactor is then heated to 550 ºC at a ramp of 10 ºC $min^{-1}$for 25 min. In this stage bypass mode is changed to reaction mode.

Session 6: Pretreatment of the catalyst at 550 ºC for 3 hours.

Session 7: After pretreatment, the feed valve of air is shut and the one regarding to N_2 is opened, feeding it at a flow rate of 15 ml min^{-1}. In this session the reactor is cooled to the reaction temperature.

3.3.2.2 Sessions for reaction

Session 8: The system is changed to bypass mode and while the reactant is fed to the reaction system for 100 min, the nitrogen feed valve is closed.

Session 9: Bypass mode is changed to reaction mode and reaction takes place at the desired reaction temperature established in session 7. The reaction lasts 15 hours but can take a little shorter depending on catalyst deactivation.

Session 10: Once the reaction has concluded, DME is not fed anymore.

Session 11: The reaction system is cooled down to room temperature.

Session 12: The whole system is shut down.

3.3.3 Reaction product analysis

For the continuous analysis of the reaction products a micro gas chromatography (Micro-GC Agilent 3000A) with 4 analytical modules has been used measuring the outlet concentration every 8 min. These modules contain a fixed inyector and a TCD detector and each one contains a different column for product separation:

- Molecular sieve (MS-5): H_2, O_2, N_2, CO and CH_4 are separated.
- Parapak Q (PPQ): CO_2, H_2O and DME are separated.

- Alumina: Paraffins and olefins are separated: Ethane, ethylene, propane, propylene, *iso*-butane, *n*-butane, *trans*-2-butene, 1-butene, *iso*-butene, *cis*-butene, *iso*-pentane, *n*-pentane, *cyclo*-pentane and pentene.
- CP-Sil 5 CB: Methanol, hexane, heptane, benzene, toluene and xylenes.

The area of each peak is proportional to the molar ratio of the component in the sample, taking into account the specific factors of the chromatographic area of each component. These factors have been obtained through a previously done measurement using a pattern with known concentration (Table 2).

Table 2. Conversion factors related to the Micro-GC Agilent 3000A.

Column	Compound	Retention time (min)	Factor (mmol area^{-1})
MS-5	CH_4	94.62	0.690
	CO	116.42	0.289
PPQ	CO_2	25.66	1.000
	DME	275.14	0.329
Alumina	Ethane	38.78	0.479
	Ethylene	40.26	0.504
	Propane	45.24	0.377
	Propylene	52.84	0.397
	Iso-butane	62.60	0.328
	n-butane	65.72	0.328
	1-butene	85.38	0.353
	Cis-butene	89.32	0.353
	trans-2-butene	94.20	0.353
	Iso-butene	100.04	0.353
	Iso-pentane	120.96	0.262
	n-pentene	131.22	0.262
	cyclo-pentane	156.70	0.262
	pentene	201.32	0.262
CP-Sil	*n*-Pentane	17.28	0.262
	Hexane	17.88	0.067
	Heptane	19.58	0.067
	Methanol	33.92	0.205
	Benzene	40.40	0.072
	Toluene	62.04	0.066
	Xylenes	101.24	0.069

After the factors have been calculated, the mmol of each product have been calculated using Equation (8). As H_2, O_2, N_2 and H_2O don't have any carbon atoms, the factors corresponding to these compounds have not been included because they are not taken into account in the calculations for the reaction indexes.

$$n_i = A\,f \tag{8}$$

where A is the area under the chromatogram and f is the conversion factor ($mmol_C\ area^{-1}$). Reaction products with similar kinetic behavior have then been grouped into different lumps. Ethane, propane, *iso*-butane and *n*-butane have been grouped into C_{2-4} paraffins; ethylene, propylene and butenes into C_{2-4} olefins; benzene, toluene and xylenes into BTX; and paraffins with more than five carbon atoms into C_{5+}.

3.4 REACTION INDEXES

In order to analyze the results obtained in the reactions, different reaction indexes have been described: 1) conversion; 2) yield of product i; 3) selectivity of product i.

1) Conversion (X) of the reaction is defined as the relationship between the difference between the outlet carbon molar flow rate of all the compounds (F_o) and the outlet carbon molar flow rate of DME (F_{DME}) and methanol (F_{MeOH}) and the outlet carbon molar flow rate of all the compounds.

$$X_i = \frac{\sum F_i - F_{DME} - F_{MeOH}}{F_{out}} 100 \tag{9}$$

2) Yield (Y_i) of product i is defined as the relationship between the carbon molar flow rate of product i (F_i) and the sum of the carbon molar flow rate of every compound in the reactor outlet, including the ones regarding the reactants (DME and methanol).

$$Y_i = \frac{F_i}{F_{out}} 100 \tag{10}$$

3) Selectivity (S_i) of product i is defined as the relationship between the carbon molar flow rate of product i and the difference between the sum of the carbon molar flow rate of every compound in the reactor outlet and the carbon molar flow rate of DME in the reactor outlet.

$$S_i = \frac{F_i}{\sum F_i - F_{DME}} 100 \tag{11}$$

4 RESULTS AND DISCUSSION

4.1 CATALYST CHARACTERIZATION

X-Ray diffraction (XRD) was used to determine the crystallinity of the materials. From the results (figure not shown), it has been verified the crystallinity of HZSM-5 and SAPO-34 catalysts. Moreover, XRD has also been used to determine the percentage of HZSM-5 and SAPO-34 in the composite catalyst. This value has been calculated from the three most intense peaks on the XRD pattern.

N_2 adsorption-desorption was used to study the porous structure of HZSM-5 and SAPO-34 catalysts. Table 3 shows the physicochemical properties of both catalysts, where the obtained values for the BET specific surface area (S_{BET}), external surface area (S_{ext}), micropore volume ($V_{micropore}$), mesopore volume ($V_{mesopore}$), total acidity and the average acid strength are displayed.

Table 3. Physicochemical properties of the catalysts.

	HZSM-5	**S-34**
Porous Structure		
S_{BET} ($m^2\ g^{-1}$)	286	408
S_{ext} ($m^2\ g^{-1}$)	135	143
$V_{micropore}$ ($cm^3\ g^{-1}$)	0.062	0.101
$V_{mesopore}$ ($cm^3\ g^{-1}$)	0.395	0.298
Acidity		
Total acidity ($mmol_{NH_3}\ g^{-1}$)	0.41	0.15
Average acid strength (kJ mol^{-1})	115	127

The results of Table 3 show that SAPO-34 catalyst has a higher surface area than that of HZSM-5 catalyst, as the S_{BET} for SAPO-34 catalyst is 408 $m^2\ g^{-1}$ comparing to 286 $m^2\ g^{-1}$ of the latter. Both catalysts present similar values for the external surface area, denoting an important presence of mesopores and macropores in the agglomerated catalyst. Nonetheless, when observing the pore volumes of each catalyst, a more important presence of mesopores stands out for the zeolite and micropores for the SAPO-34 catalyst. This explains the higher specific surface area determined for the second catalyst.

The acidity of the catalysts was studied by adsorption-desorption of NH_3, where HZSM-5 catalyst presents a higher total acidity value (0.41 $mmol_{NH_3}\ g^{-1}$) than that corresponding to SAPO-34 (0.15 $mmol_{NH_3}\ g^{-1}$) catalyst. Nevertheless, the acid sites of the SAPO-34 show a stronger character than those of HZSM-5, as the average acid strength values are higher (127 and 115 kJ mol^{-1} for SAPO-34 and HZSM-5, respectively).

4.2 KINETIC PERFORMANCE OF HZSM-5

In this chapter the effect of two important operating variables (space time and temperature) over the reaction indexes previously stated in section 3.4 has been studied. The study was carried out using HZSM-5 zeolite (SiO_2/Al_2O_3 = 15) agglomerated with boehmite (γ-Al_2O_3 once it was calcined) and α-Al_2O_3.

The operating conditions were: pressure, 1.4 bar; temperature, 350–400 ºC; space time, 1–2 g_{cat} h mol_C^{-1}; time on stream (TOS), 15 h. It must be noted that in this and the next chapters, space time is referred to the catalyst mass and that zero time on stream corresponds to 8 min after reaction has started in order to avoid the inaccuracy of results during the stabilization period of the reaction.

4.2.1 Effect of space time

The yields of different lumps (C_{2-4} olefins, C_{2-4} paraffins, BTX and C_{5+}) at zero TOS with space time values of 1 and 2 g_{cat} h mol_C^{-1} are shown in Figure 6. The reactions were carried out at 350 ºC with DME feed.

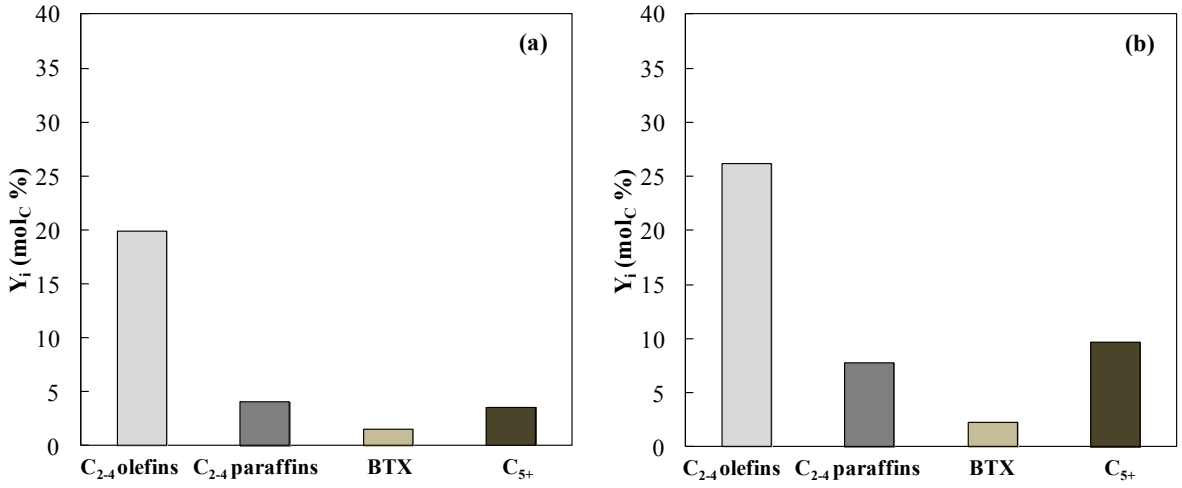

Figure 6. Comparison of yields of different lumps at zero time on stream using space time of (a) 1 and (b) 2 g_{cat} h mol_c^{-1} at 350 ºC.

As observed in Figure 6, the yields of C_{2-4} paraffins, BTX and C_{5+} increase from 4, 1.5 and 3.5% to 8, 2 and 10%, respectively, upon increasing the space time. Secondary reactions start taking place when increasing the space time, being the most important ones the hydrogen transfer and aromatization reactions. These reactions are multistage and/or bimolecular reactions, therefore, they are favored with increasing contact time (Choudhary et al., 2002).

A higher increase on the yield of alkanes C_{5+} comparing to aromatics when increasing the space time is interesting, because this lump is susceptible to the selective cracking of olefins (Pérez-Uriarte et al., 2016a), allowing its recirculation on an industrial reactor. This limitation on the yields of aromatics can be attributed to the low acidity and average acid strength of the catalyst compared to other similar catalysts used in previous researches.

Furthermore, the selectivities of the desired olefins (C_2H_4, C_3H_6 and C_4H_8), CH_4, methanol and $CO+CO_2$ at zero TOS with space time values of 1 and 2 g_{cat} h mol_C^{-1} are shown in **Figure 7**a and 7b. The reactions were carried out in the operating conditions aforementioned.

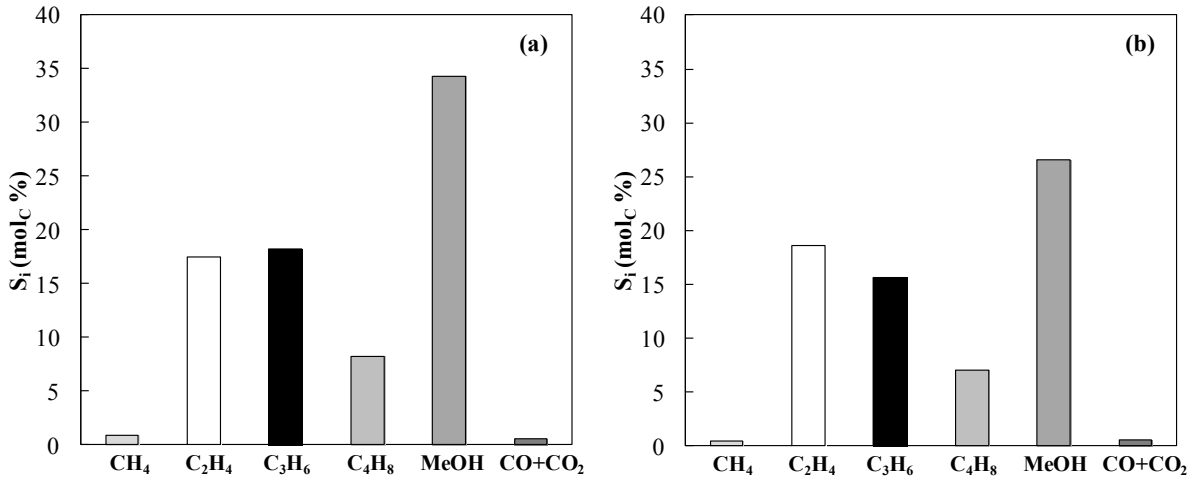

Figure 7. Comparison of selectivities of products at zero TOS using space time of: (a) 1 and (b) 2 g_{cat} h mol_c^{-1} at 350 ºC.

As it can be seen when comparing Figure 7a and 7b, space time plays an important role in the selectivity of light olefins. On the one hand, an increase in the space time drops the selectivity of propylene, which is the primary product, from 18 to 15%. On the other hand, the selectivity of ethylene increases from 17 to 19% because ethylene needs higher space time values in order to be reactive in oligomerization-cracking reactions due to the limited acidity of the catalyst. These results are consistent with those reported by Perez-Uriarte (2016a) who explains that propylene suffers a steady decrease on its selectivity when increasing the space time whereas selectivity of ethylene goes through a maximum. Like propylene, selectivity of butenes drops when increasing the space time values. This is related to ethylene formation from butenes, as increasing the space time value increases the reactivity of butenes cracking to ethylene. This behavior would explain the decrease in the selectivity of butenes and the increase in selectivity of ethylene. Otherwise, the selectivity of methanol suffers a major decrease from 34 to 26% because the higher conversion of oxygenated upon increasing the space time favors reactions to form C_{5+} aliphatic, BTX and light alkanes.

4.2.2 Effect of temperature

Figure 8 displays the yields of the main reaction product lumps (C_{2-4} olefins, C_{2-4} paraffins, BTX and C_{5+}) at zero TOS at 350 and 400 ºC. The reactions were carried out with a space time value of 1 g_{cat} h mol_C^{-1} with DME feed.

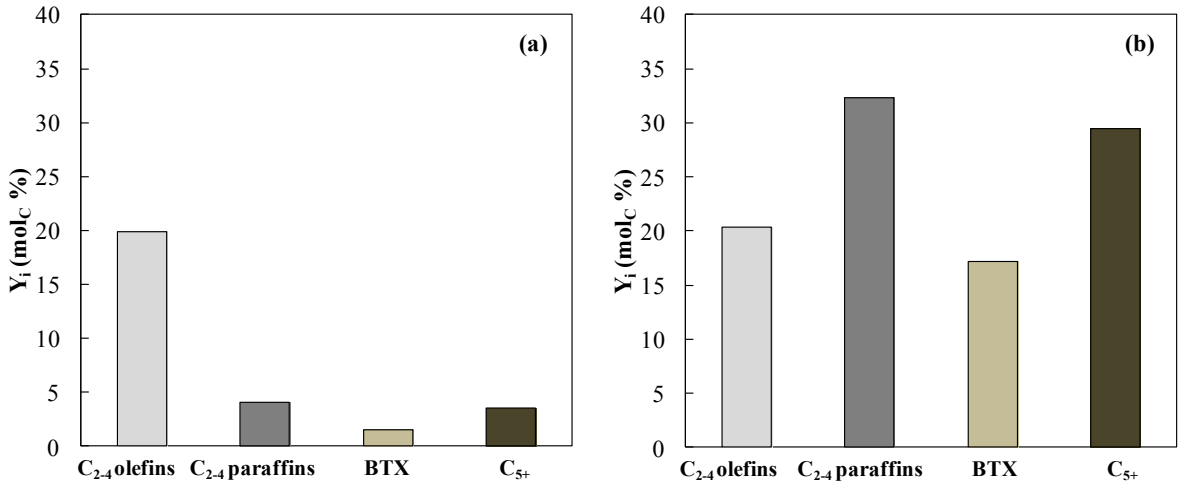

Figure 8. Comparison of yields of different lumps at zero TOS for HZSM-5 catalyst. Reaction conditions: Temperature, (a) 350 and (b) 400 ºC; space time, 1 g_{cat} h mol_C^{-1}.

Yields corresponding to C_{2-4} paraffins, BTX and C_{5+} are strongly affected by temperature, as an increasing the temperature from 350 to 400 ºC increases the yields from 4, 1.5 and 3% to 32, 17 and 29%, respectively (Figure 8). On the other hand, yield of C_{2-4} olefins seems to remain unaffected as it remains constant at around 20%. These results are explained by the promotion of secondary reactions on the acidic sites when increasing the temperature. This way, endothermic reactions like olefin oligomerization and condensation to aromatics are favored, resulting in an increase on heavier hydrocarbon species. Moreover, formation of paraffins from olefins due to hydrogen transfer also takes place at higher temperatures, because they are not limited by thermodynamic constraints at these low temperatures.

The selectivities of the desired olefins, CH_4, methanol and $CO+CO_2$ at zero TOS at 350 ºC and 400 ºC are shown in Figure 9a and 9b. The reaction was carried out with DME feed and a space time value of 1 g_{cat} h mol_C^{-1}.

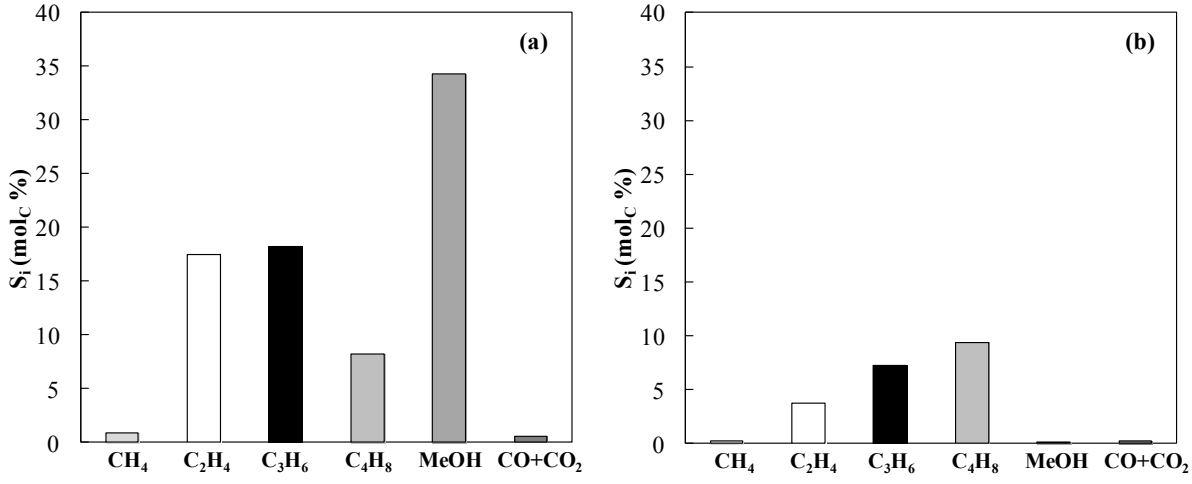

Figure 9. Comparison of selectivities of the desired products at zero TOS for HZSM-5 catalyst. Reaction conditions: Temperature, (a) 350 and (b) 400 ºC; space time, 1 g_{cat} h mol_C^{-1}.

Selectivity of both propylene and ethylene is very negatively affected with increasing the temperature from 350 to 400 ºC as a steady decrease from 18 and 17% to 7 and 4% is appreciated (Figure 9). This could be attributed to the high reactivity of propylene for oligomerization-cracking reactions and its exclusive primary product nature. By contrast, selectivity of ethylene increases with increasing temperatures up to 350 ºC, followed by a decrease in selectivity if the temperature is increased further more (Pérez-Uriarte et al., 2016) which is in accordance with our results. This can be related to the lower reactivity of ethylene comparing to propylene when it comes to oligomerization-cracking reactions. As reactivity of butenes is very low, its selectivity remains constant with temperature.

The selectivity of CH_4 is low at both temperatures (less than 1% for both operating temperatures). This is related to the origin of CH_4, which is only obtained by thermal cracking. When increasing the temperature, the catalytic reactions with high activation energy that compete with thermal cracking are favored, thus resulting in low selectivity of CH_4. Nevertheless, even though thermal cracking is less important than catalytic reactions at higher temperatures, it must be noted that the higher the temperature the more CH_4 will be obtained. Furthermore, the low selectivity of CO and CO_2 for both temperatures endorses the theory that catalytic reactions are favored at these temperatures, as CO and CO_2 are direct products of thermal cracking of DME.

Selectivity of methanol is strongly affected by temperature, as it decreases from 35% at 350 ºC to 1% at 400 ºC. At 350 ºC, conversions of around 30% for space time values of 1 g_{cat} h mol_C^{-1} are achieved at zero TOS, whereas at 400 ºC, conversion values of almost 100% are obtained for the same operating conditions. This difference in conversions accounts for the difference in the selectivity of methanol, where at higher temperatures the pool of DME and methanol reacts to form paraffins, BTX and aliphatic C_{5+}.

4.3 SAPO-34

The performance of the HZSM-5 based catalyst has been compared with that of a SAPO-34 based catalyst, as it is the one used at industrial scale. The space time values generally used with this catalyst are much greater than those shown previously for the HZSM-5 catalyst. For this reason and with the objective of making a comparison of the catalysts within a similar yield range, a space time of 24 g_{cat} h mol_C^{-1} has been used for SAPO-34 catalyst. The yields of different lumps and the selectivity of olefins as well as other compounds at zero TOS at 350 ºC are shown in Figure 10.

Comparing the yields obtained using the SAPO-34 catalyst (Figure 10a) and the HZSM-5 catalyst (Figure 8a), it can be stated that smaller yields are obtained with SAPO-34 catalyst for every lump at 350 ºC with space time values much higher than those used with HZSM-5 catalyst. This is related with the lower conversion obtained with the SAPO-34 based catalyst despite the higher space time used. Furthermore, the formation of BTX and C_{5+} is negligible using SAPO-34 catalyst, whereas yields of up to 3 and 10% are acquired for HZSM-5 catalyst. This trend is also followed with both olefins and paraffins, where yields up to 20 and 8% are obtained for HZSM-5 catalyst and 12 and 3% for SAPO-34 catalyst.

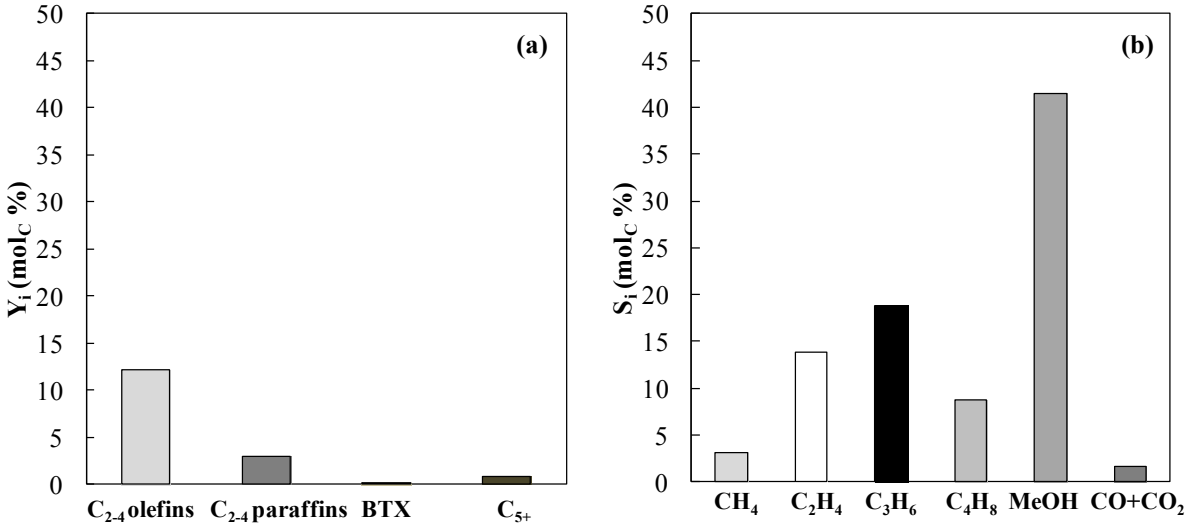

Figure 10. Comparison of (a) yields of different lumps and (b) selectivities of the desired products at zero TOS for SAPO-34 catalyst. Reaction conditions: Temperature, 350 ºC; space time, 24 g_{cat} h mol_c^{-1}.

Despite the difference on the yields, the selectivities for HZSM-5 (Figure 9a) and SAPO-34 (Figure 10b) catalysts are very similar, 17 and 14% for ethylene, 18 and 19% for propylene and 8 and 9% for butene, respectively. These similarities in selectivities suggest that both catalysts present appropriate shape selectivity for the production of light olefins. Moreover, propylene is the main olefin product in both cases, which is the olefin with higher demand as we previously mentioned in the introduction section. However, the much higher activity of HZSM-5 catalyst leads to a higher production of olefins but mixed with undesirable BTX or C_{5+} products.

4.4 CATALYST DEACTIVATION

The evolution of conversion of DME at 350 ºC (previously defined in Equation 9) along the TOS is shown in Figure 11a. The study has been done for both HZSM-5 and SAPO-34 catalysts, where very different behavior can be observed in both cases. In spite of the space time value for SAPO-34 catalyst being an order of magnitude higher than that of HZSM-5 catalyst, the catalyst presents a basically total deactivation after 10 min of reaction. On the other hand, the HZSM-5 catalyst shows a slower drop in activity with the time on stream. As it can be seen in Figure 11a, an increase on the space time of HZSM-5 catalyst implies an increase on the initial conversion (50 and 30% respectively). Nevertheless, a similar deactivation trend is observed for both catalysts at 10 h TOS.

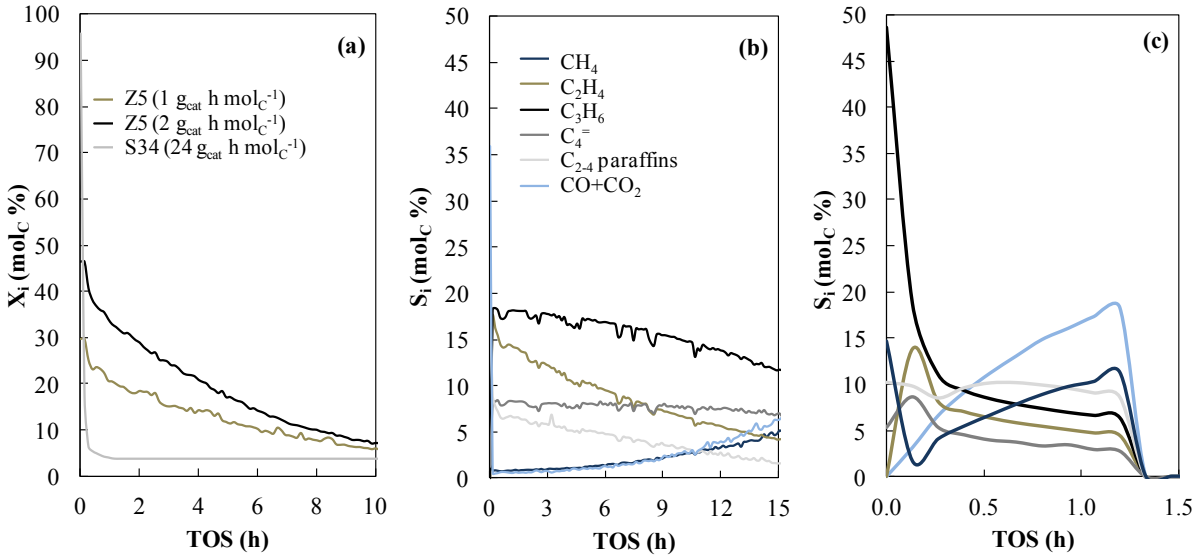

Figure 11. Evolution on TOS of: (a) conversion of DME; (b) selectivity of reaction products with HZSM-5 zeolite; (c) selectivity of reaction products with SAPO-34 catalyst (T = 350 ºC)

In Figure 11b and 11c, the evolution of the selectivities of the reaction products for HZSM-5 catalyst at 350 ºC and space time value of 1 g_{cat} h mol_C^{-1} and for SAPO-34 catalyst at 350 ºC and space time value of 24 g_{cat} h mol_C^{-1} is displayed. As it can be seen in Figure 11b, olefins have the highest selectivities among the reaction products, propylene being the main one when HZSM-5 is used as catalyst. The loss on the catalyst activity supposes a decrease on the selectivity of ethylene and an increase on the selectivity of butene, which could probably be due to the lower reactivity of butenes that do not crack on the remaining acid sites of the partially deactivated catalyst. On the same way, the selectivity of paraffins decreases as the density of strong acid sites that promote the hydrogen transfer reactions decreases.

In Figure 11c it is observed how very high selectivity of olefins is achieved at small times when SAPO-34 is used as catalyst. On the other hand, the selectivity of paraffins remains constant at around 10%. The deactivation of the catalyst causes thermal cracking reaction to increase, thus increasing the selectivities of both methane and $CO+CO_2$. This phenomenon is also observed when using HZSM-5 catalyst after 10 hours TOS (Figure 11b).

The results from Figure 11 are related to the different porous structure of the catalysts. The small size of the pore and box system of the SAPO-34 causes a high shape selectivity of small lineal olefins but does not allow the BTXs to spread towards the exterior of the crystals of the zeolite. In this way, the aromatics that are formed according to the double cycle mechanism (hydrocarbon pool) that follows the transformation of DME to olefins condense on the acid sites of the SAPO-34 catalyst. On the other hand, the straight and bigger size channels of HZSM-5 catalyst allow the diffusion of the BTX compounds, thus minimizing the formation of coke on the acid sites of the catalyst (Epelde et al., 2014).

This result shows that working with SAPO-34 would require using very short residence times for the catalyst, in order to get considerable olefin production results. On the other hand, the

larger stability of HZSM-5 catalyst allows working with higher TOS as well as increasing the space time (10–20 times less than SAPO-34 catalyst). Because of this, the SAPO-34 catalyst should be used in a fluidized bed reactor in cycles with a combustor/regenerator and using short residence times. Nevertheless, the HZSM-5 catalyst allows to operate on both the system aforementioned and fixed bed reactor using high TOS and space times, obtaining considerable yields of olefins.

In order to characterize the amount and nature of the coke deposited on the catalyst surface during the transformation of DME into olefins, temperature programmed oxidation (TPO) analyses were carried out. The TPO profiles for 350 and 400 ºC are displayed in Figure 12a and 12b. The coke content can be determined from the area under the curve and the nature and/or localization from the temperature of the maximum.

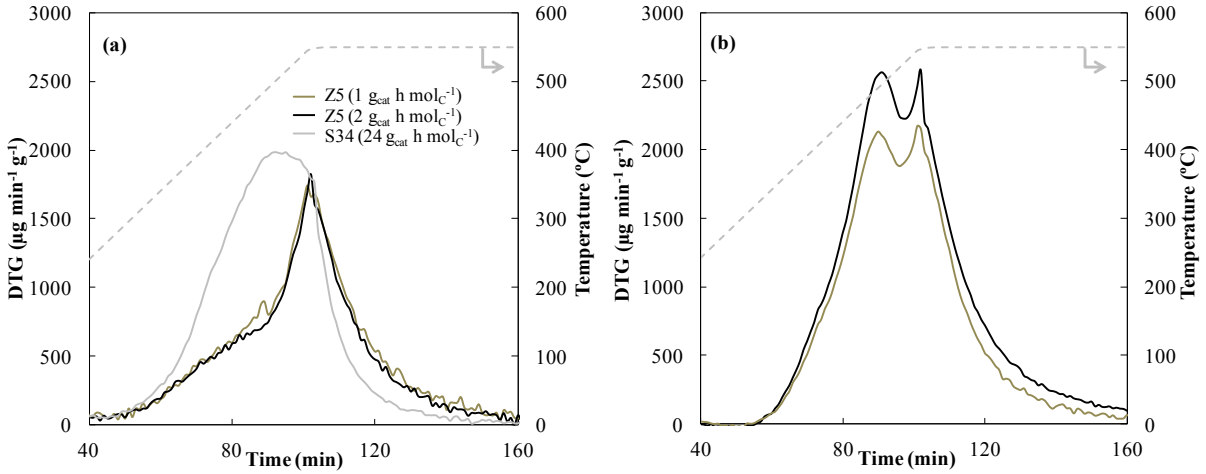

Figure 12. TPO profiles of the deactivated catalysts at (a) 350 and (b) 400 ºC.

On the one hand, it can be deduced that SAPO-34 catalyst has a coke with heterogeneous nature due to the wider profile of its TPO curve (Figure 12a). This could also indicate that the SAPO-34 catalyst shows bigger diffusional problems in combustion of coke owing to its structure of boxes and channels (Epelde et al., 2014). On the other hand, HZSM-5 catalyst shows a narrower TPO profile, and it is independent of space time at low temperatures. Moreover, the temperature of the maximum implies that the structure of the coke is presumably more developed (Le Minh et al., 1997).

The study of the TPO profiles of only the HZSM-5 catalyst has been done at high temperatures, as seen in Figure 12b. In this case, the effect of space time is noticeable, as an increase on the space time also increases the amount of coke. The TPO profile shows two well-defined peaks, which indicates the presence of two different species of coke. This could be related to the different nature or location of the coke. On the one hand, the peak with maximum at T = 480 ºC can be associated with a less developed coke, with a higher H/C ratio and that it is presumably deposited on the mesoporous matrix of the alumina. The second peak with maximum at T = 550 ºC can be associated to a more condensed coke that is deposited on the micropores of the crystalline structure of the HZSM-5 catalyst (Valle et al., 2012).

Table 4 summarizes the content of coke of each of the catalysts used in this work. As it can be seen, the amount of coke increases upon increasing the reaction temperature in the HZSM-5 based catalyst. This result suggests that the condensation reactions of BTX aromatics for yielding polyaromatic structures of coke are favored when the temperature is increased. This is also consistent with the faster deactivation observed at this temperature for the HZSM-5 catalyst (figure not shown). At these conditions, the catalyst shows a total deactivation after 5 and 6 h TOS for the HZSM-5 catalyst when using a space time of 1 and 2 g_{cat} h mol_C^{-1}, respectively.

Table 4. Amount of coke in the deactivated catalysts.

	350 ºC (wt%)	**400 ºC (wt%)**
HZSM-5 (τ=1 g_{cat} h mol_C^{-1})	6.71	8.71
HZSM-5 (τ=2 g_{cat} h mol_C^{-1})	6.30	10.00
SAPO-34 (τ=24 g_{cat} h mol_C^{-1})	9.36	-

Regarding the amount of coke deposited on the HZSM-5 and SAPO catalysts at 350 ºC, a noticeable increase of coke is observed for SAPO-34 catalyst. These results are consistent with the faster deactivation observed in Figure 11a, and are related with the previously discussed low yield of BTX aromatics when using the SAPO-34 catalyst (Figure 10a). All these results are explained by the different shape selectivity of the catalyst and are schematized in Figure 13.

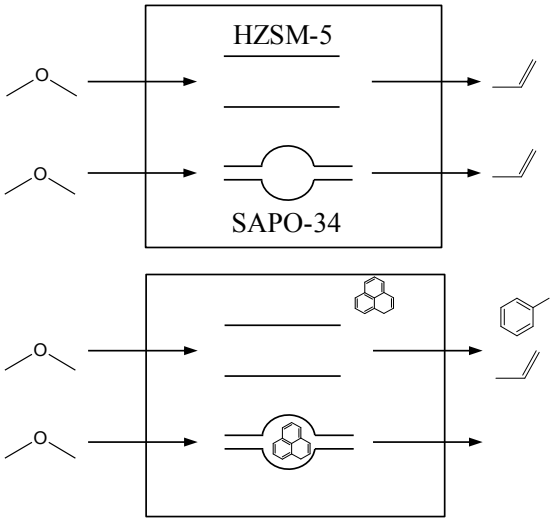

Figure 13. Scheme of DTO reaction over HZSM-5 and SAPO-34 catalysts.

As observed, the channels of both catalysts show appropriate size in order to yield light olefins. In addition, the straight and bigger channels of HZSM-5 allow the diffusion of BTX aromatics and coke precursor to the mesoporous matrix. In this way, BTX aromatics are observed as reaction products and coke is presumably deposited on the matrix surface. However, the smaller size of the channel of the SAPO-34 avoids the diffusion of BTX aromatics and leads to the formation of polyaromatic structures inside the cages of the silicoaluminophosphate, which lead to a faster catalyst deactivation.

4.5 COMPOSITE

In this section, the performance of a composite catalyst (C5) formed by HZSM-5 and SAPO-34 active phases is evaluated. The catalyst, prepared through physical blending, has the suitable proportion of each active phase in which the contribution of both phases should be noted. The conversions along the time on stream of C5, HZSM-5 and SAPO-34 are displayed in Figure 14a, and the obtained selectivities of methane, olefins, paraffins and $CO+CO_2$ with each catalyst above mentioned are shown in Figure 14b, 14c and 14d, respectively. The reaction was carried out at 375 ºC with DME feed and space time values of 0.5, 9.5 and 10 g_{cat} h mol_C^{-1} for HZSM-5, SAPO-34 and C5 catalysts. These individual space time values correspond to the relative mass of HZSM-5 and SAPO-34 in C5 composite catalyst.

Figure 14a shows the evolution of conversion with the TOS. The composite shows a very high initial conversion just like SAPO-34 catalyst, but the decrease observed on the SAPO-34 is not appreciated on the composite material. In this regard, after conversion values of 60% the decrease is slower than that of SAPO-34 catalyst and resembles to that of HZSM-5 catalyst. Additionally, it can be seen how for practically every TOS the conversion of the composite is superior to the sum of the individual conversions (SAPO-34 catalyst presents a constant conversion until 10 hours TOS). This result demonstrates the synergy between both phases of the catalyst, showing that the use of both phases in a composite improves the activity and stability of the catalyst.

Figure14b, 14c and 14d show the selectivities of the products of the different catalysts. The composite C5 catalyst (Figure 14b) shows a product distribution similar to that of the HZSM-5 catalyst (Figure 14c), observing similar trends for all the reaction products. Nevertheless, during the first minutes of reaction maximum selectivity of olefins is observed, which coincides with that of SAPO-34 catalyst (Figure 14d). The maximum selectivity takes place at the same TOS value for both catalysts, the time being 10 min. In this way, the composite shows maximum selectivities of ethylene, propylene and butenes of 20, 25 and 13%. These values are similar to the values obtained by summing the one obtained with each catalyst individually. In conclusion, and taking into account that the conversion is also much higher in the composite, is possible to conclude that the production of olefins is much higher in C5 composite catalyst than in the individual catalysts.

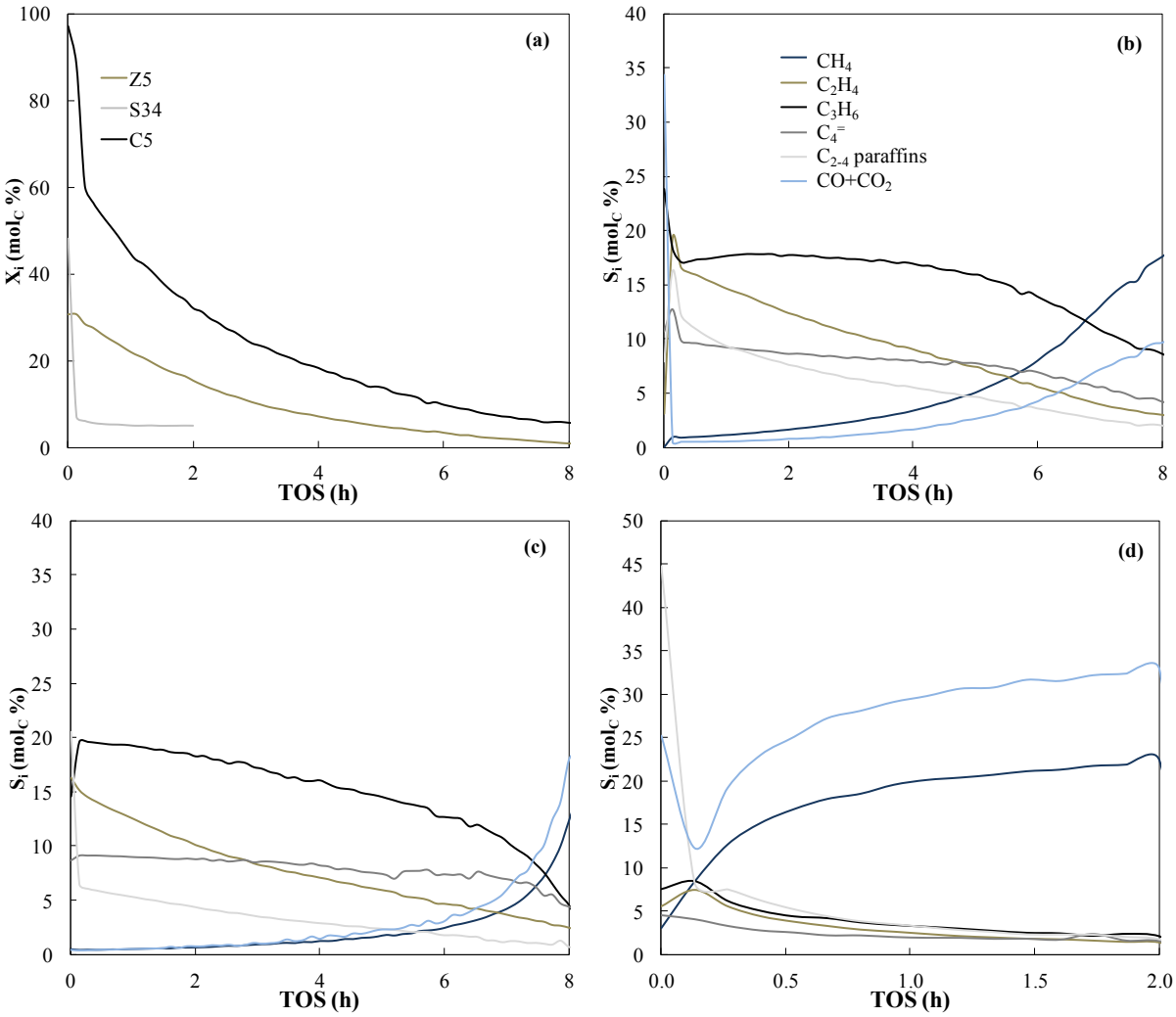

Figure 14. Evolution on TOS of: (a) conversion of DME; (b) selectivity of reaction products with C5; (c) selectivity of reaction products with HZSM-5 catalyst; (d) selectivity of reaction products with SAPO-34 catalyst (T = 350 ºC).

The results of figure 14 prove a synergic effect of both phases (HZSM-5/SAPO-34) regarding the results of each individual phase. In this regard, the composite presents similar selectivities of olefins comparing to those obtained from HZSM-5 and SAPO-34 catalysts individually, but it is much more stable along the TOS than the SAPO-34 catalyst and shows olefins maximum on the product distribution comparing to HZSM-5 catalyst. The influence of the SAPO-34 catalyst has been seen during small TOS, with high conversions giving rise to maximums in selectivities of olefins and a rapid decrease on the activity of the catalyst. On the other hand, the effect of the HZSM-5 catalyst is visible during long TOS, with a slower decrease in conversion, which contributes the catalyst with higher stability and maintains sufficiently high values for selectivity of olefins.

5 CONCLUSIONS

- Different catalysts have been prepared by binding the acid phases (SAPO-34 and HZSM-5) with boehmite and α-Al_2O_3, providing it with a hierarchical porous structure with a mesopore matrix that comprised the crystals of the acid function. This gives both mechanical and hydrothermal resistance to the catalyst and contributes to mitigate the deactivation of the catalyst produced by the blockage of the micropores with coke.

- Regarding the structural properties of the catalysts, SAPO-34 shows a higher specific surface area (S_{BET}) but a lower pore volume than HZSM-5, denoting a major presence of mesopores for HZSM-5 catalyst and micropores for the SAPO-34 catalyst. This result is in accordance with the values obtained for the specific surface area. However, the external surface area (S_{ext}) is similar for both catalysts and indicates the importance of the mesoporous structure that is embedded on the γ-Al_2O_3 matrix.

- Space time has been determined to be an important factor in the conversion of dimethyl ether into olefins as increasing it favors secondary reactions forming BTX, C_{5+} aliphatics and paraffins while the yield of olefins barely increases. Furthermore, increasing the temperature from 350 to 400 ºC brings along a steady decrease of the selectivities of olefins, specially propylene, due to its high reactivity, and, in contrast, a significant increase of the yields of BTX, C_{5+} aliphatic and C_{2-4} paraffins due to hydrogen transfer and oligomerization-cracking reactions. Full conversions of DME are obtained at 400 ºC and 1 g_{cat} h min^{-1}, leading to more unwanted products (saturated compounds).

- SAPO-34 catalyst has shown a selectivity of propylene of 19% and a fast deactivation (only lasting 10 min) caused by the pore blockage due to the alkylated aromatics depositing on the internal cages of channel intersections. On the other hand, HZSM-5 catalyst shows lower propylene selectivity (18%) and a slower deactivation rate as these alkylated aromatics are swept away to the outside of the micropores, depositing on the mesopores of the matrix and avoiding the blockage of the catalytic acid sites. The higher diameter of the micropores of HZSM-5 compared with SAPO-34 catalysts, and the absence of cages in the former, also enable the external deposition of the coke.

- The fast deactivation of the SAPO-34 catalyst and high space time values compared to HZSM-5 catalyst suggest that if it is wanted to use industrially, this must be done in a fluidized bed reactor with a combustor/regenerator to avoid deactivation, and always using small residence time values. However, HZSM-5 can be used in both fluidized and fixed bed reactors, using high TOS and space times.

- The synergic effect of HZSM-5 and SAPO-34 is proven in a composite catalyst, as the selectivities of olefins are similar to those obtained for each individual catalyst. However, the composite catalyst shows higher stability than the SAPO-34 along the time on stream and olefins maximum on the product distribution that the HZSM-5 catalyst does not show. The effect of SAPO-34 is observed at short TOS, whereas the influence of the zeolite is present at high values of TOS. Furthermore, the conversion for the composite catalyst is determined to be higher than the sum of the conversions of the individual active phases.

6 NOMENCLATURE

A	Area under the chromatogram, area
d	Interplanar distance, nm^{-1}
f	Conversion factor, $mmol_C\ area^{-1}$
F_{DME}	Carbon molar flow rate of DME in the reactor outlet, $mol_c\ min^{-1}$
F_i	Carbon molar flow rate of lump i in the reactor outlet, $mol_c\ min^{-1}$
F_{MeOH}	Carbon molar flow rate of MeOH in the reactor outlet, $mol_c\ min^{-1}$
F_o	Total carbon molar flow rate of DME in the reactor outlet, $mol_c\ min^{-1}$
n	Interger, dimesionless
n_i	Moles of product i, mmol
T	Temperature, ºC
S_i	Selectivity of product i, %
X	Conversion, %
Y_i	Yield of lump i, %

6.1 GREEK LETTERS AND SYMBOLS

λ	Wavelength of the incipient ray, nm^{-1}
θ	Diffraction angle, degrees
τ	Space time, $g_{cat}\ h\ mmol_C^{-1}$

6.2 ACHRONIMS AND ABBREVIATIONS

BET	Brunauer Emmet Teller
C5	Composite catalyst containing 5% HZSM-5 zeolite
DME	Dimethyl ether
DOMY	Dimethyl oxonium methyl ylide
DTO	Dimethyl ether to Olefins
FCC	Fluid Catalytic Cracking
GC	Gas Chromatography
HCP	Hydrocarbon Pool
LPG	Liquefied Petroleum Gas
MFI	Mordenite Inverted Framework
MTO	Methanol to Olefins
MTP	Methanol to Propylene
PDH	Propane Dehydrogenation
PE	Polyethylene
PP	Polypropylene
SAPO	Silicoaluminophosphate
SMS	Surface Methoxy Species
STD	Syngas to Dimethyl ether

STP	Standard Temperature and Pressure (0 ºC, 1 bar). Used as a subscript: "STP"
TG-TPO	Themrogravimetric-Temperature Programmed Oxidation
TMO	Trimethyl oxonium
TOS	Time on stream
TPD	Temperature Programmed Desorption
WGS	Water Gas Shift
XRD	X-Ray Diffraction

7 REFERENCES

Abramova, A.V., 2009. Development of catalysts based on pentasil-type zeolites for selective synthesis of lower olefins from methanol and dimethyl ether. Catal. Ind. 1, 267-277.

Al-Dughaither, A.S., 2014. Conversion of Dimethyl ether to Olefing over HZSM-5: Reactivity and Kinetic Modeling. Doctoral Dissertation, University of Western Ontario.

Al-Dughaither, A.S., De Lasa, H., 2014. Neat Dimethyl ether Conversion to Olefins (DTO) over HZSM-5: Effect of SiO_2/Al_2O_3 on Porosity, Surface Chemistry and Reactivity. Fuel 15, 52-64.

AlWahabi, S., 2003. Conversion of Methanol to Light Olefins on Sapo-34 Kinetic Modeling and Reactor Design. Doctoral Dissertation, Texas A&M University, Dept. of Chemical Engineering.

Arcoumanis, C., Bae, C., Crookes, R., Kinoshita, E., 2008. The potential of di-methyl ether (DME) as an alternative fuel for compression-ignition engines: A review. Fuel 87, 1014-1030.

Azizi, Z., Rezaeimanesh, M., Tohidian, T., Rahimpour, M.R., 2014. Dimethyl ether: A review of technologies and production challenges. Chem. Eng. Process. 82, 150-172.

Bjørgen, M., Lillerud, K.P., Olsbye, U., Svelle, S., 2007. Conversion of methanol to hydrocarbons: Hints to rational catalyst design from fundamental mechanistic studies on H-ZSM-5. Stud. Surf. Sci. Catal. 167, 463-468.

Čejka, J., Bekkum, H.V., 2005. Zeolites and ordered mesoporous materials. Elsevier.

Chemsystems. 2007. Olefins outlook positive until 2009. Retrieved June 21, 2017, from http://database.thinking.nexant.com/about/cs/news/items/Olefins%20Market%20Dynamics.cfm.

Chen, W.H., Hsu, C.L., Wang, X.D., 2016. Thermodynamic approach and comparison of two-step and single step DME (dimethyl ether) syntheses with carbon dioxide utilization. Energy 109, 326-340.

Chen, W.H., Lin, B.J., Lee, H.M., Huang, M.H., 2012. One-step synthesis of dimethyl ether from the gas mixture containing CO_2 with high space velocity. Appl. Energ. 98, 92-101.

Chenier, P., 2002. Survey of Industrial Chemistry, 3rd ed. Kluwer Academic, New York.

Chowdhury, A.D., Houben, K., Whiting, G.T., Mokhtar, M., Asiri, A.M., Al-Thabaiti, S.A., Basahel, S.N., Baldus, M., Weckhuysen, B.M., 2016. Initial Carbon–Carbon Bond Formation during the Early Stages of the Methanol-to-Olefin Process Proven by Zeolite-Trapped Acetate and Methyl Acetate. Angew. Chem. Int. Ed. 128, 16072-16077.

Curtis, N., Kang, S.C., Choi, S., Oh, S.H., Park, Y.K., 2007. A catalytic cracking process for ethylene and propylene from paraffin streams: the Advanced Catalytic Olefins (ACO) Process. AIChE spring national meeting, Houston, Texas.

Duan, C., Zhang, X., Zhou, R., Hua, Y., Chen, J., Zhang, L., 2011. Hydrothermally synthesized HZSM-5/SAPO-34 composite zeolite catalyst for ethanol conversion to propylene. Catal. Lett. 141, 1821-1827.

Duan, C., Zhang, X., Zhou, R., Hua, Y., Zhang, L., Chen, J., 2013. Comparative studies of ethanol to propylene over HZSM-5/SAPO-34 catalysts prepared by hydrothermal synthesis and physical mixture. Fuel Process. Technol. 108, 31-40.

Epelde, E., Ibañez, M., Aguayo, A.T., Gayubo, A.G., Bilbao, J., Castaño, P., 2014. Differences among the deactivation pathway of HZSM-5 zeolite and SAPO-34 in the transformation of ethylene or 1-butene to propylene. Microporous Mesoporous Mater. 195, 284-293.

Ereña, J., Sierra, I., Aguayo, A.T., Ateka, A., Olazar, M., Bilbao, J., 2011. Kinetic modelling of dimethyl ether synthesis from (H_2+CO_2) by considering catalyst deactivation. Chem. Eng. J. 174, 660-667.

Ghavipour, M., Mosayebi, R., Beagherian, R., Samadi, A., 2014. Methanol/dimethyl ether to light olefins over SAPO-34: Comprehensive comparison of the products distribution and catalyst performance. J. Nat. Gas Sci. Eng. 21, 532-539.

Gil-Coba, J., Marie-Rose, S.C., Lavoie, J.M., 2016. Effect of Water Content and Catalysts Acidity in the Products Distribution During Propylene Synthesis with a Mixture of DME and Methanol. Catal. Lett. 146, 2534-2542.

Fleisch, T.H., Basu, A., Sills, R.A., 2012. Introduction and advancement of a new clean global fuel: The status of DME developments in China and beyond. J. Nat. Gas Sci. Eng. 9, 94-107.

Froment, G., Dehertog, W., Marchi, A., 1992. Zeolite catalysis in the conversion of methanol into olefins. Catal. Today 9, 1-64.

Hua, Y., Guo, X., Mao, D., Lu, G., Rempel, G.L., Ng, F.T., 2017. Single-step synthesis of dimethyl ether from biomass-derived syngas over CuO-ZnO-MO x (M= Zr, Al, Cr, Ti)/HZSM-5 hybrid catalyst: Effects of MO x. Appl. Catal., A 540, 68-74.

Jiang, Y., Wang, W., Marthala, V.R., Huang, J., Sulikowski, B., Hunger, M., 2006. Effect of organic impurities on the hydrocarbon formation via the decomposition of surface methoxy groups on acidic zeolite catalysts. J. Catal. 238, 21-27.

Keil, F.J., 1999. Methanol-to-hydrocarbons: process technology. Microporous Mesoporous Mater. 29, 49-66.

Koempel, H., Liebner, W., 2007. Lurgi's Methanol To Propylene (MTP) Report on a successful commecialisation. Stud. Surf. Sci. Catal. 167, 261-267.

Ladera, R., Finocchio, E., Rojas, S., Fierro, J.L.G., Ojeda, M., 2012. Supported niobium catalysts for methanol dehydration to dimethyl ether: FTIR studies of acid properties. Catal. Today 192, 36-143.

Le Minh, C., Jones, R.A., Craven, I.E., Brown, T.C., 1997. Temperature-programmed oxidation of coke deposited on cracking catalysts: combustion mechanism dependence. Energy Fuels 11, 463-469.

Lei, Z., Zou, Z., Dai, C., Li, Q., Chen, B., 2011. Synthesis of dimethyl ether (DME) by catalytic distillation. Chem. Eng. Sci 66, 3195-3203.

Lok, B.M., Messina, C.A., Patton, R.L., Gajek, R.T., Cannan, T.R., Flanigen, E.M., 1984. Silicoaluminophosphate molecular sieves: another new class of microporous crystalline inorganic solids. J. Am. Chem. Soc. 106, 6092-6093.

Markets and Markets. (n.d.). Dimethyl Ether Market worth 9.7 Billion USD by 2020. Retrieved June 21, 2017, from http://www.marketsandmarkets.com/PressReleases/dimethyl-ether.asp.

Michels, N.L., Mitchell, S., Pérez-Ramírez, J., 2014. Effects of binders on the performance of shaped hierarchical MFI zeolites in methanol-to-hydrocarbons. ACS Catal. 4, 2409-2417.

Mulla, S., Buyevskaya, O., Baerns, M., 2002. A comparative Atudy on Non-Catalytic and Catalytic Oxidative Dehydrogenation of Ethane to Ethylene. Appl. Catal., A 226, 72-78.

Nováková, J., Kubelková, L., Dolejšek, Z., 1987. Primary reaction steps in the methanol-to-olefin transformation on zeolites. J. Catal. 108, 208-213.

Olah, G.A., 2005. Beyond Oil and Gas: The Methanol Economy. Angew. Chem. Int. Ed. 18, 2636-2639.

Olah, G.A., Doggweiler, H., Felberg, J.D., Frohlich, S., Grdina, M.J., Karpeles, R., Keumi, T., Inaba, S.I., Ip, W.M., Lammertsma, K., Salem, G., 1984. Onium Ylide chemistry. 1. Bifunctional acid-base-catalyzed conversion of heterosubstituted methanes into ethylene and derived hydrocarbons. The onium ylide mechanism of the C1. fwdarw. C2 conversion. J. Am. Chem. Soc. 106, 2143-2149.

Olsbye, U., Svelle, S., Lillerud, K.P., Wei, Z.H., Chen, Y.Y., Li, J.F., Wang, J.G., Fan, W.B., 2015. The formation and degradation of active species during methanol conversion over protonated zeotype catalysts. Chem. Soc. Rev. 44, 7155-7176.

Park, Y.K., Lee, C.W., Kang, N.Y., Choi, W.C., Choi, S., Oh, S.H., Park, D.S., 2010. Catalytic cracking of lower-valued hydrocarbons for producing light olefins. Catal. Surv. Asia 14, 75-84.

Perez-Uriarte, P., Ateka, A., Aguayo, A.T., Gayubo, A.G., Bilbao, J., 2016a. Kinetic model for the reaction of DME to olefins over a HZSM-5 zeolite catalyst. Chem. Eng. J. 302, 801-810.

Perez-Uriarte, P., Gamero, M., Ateka, A., Diaz, M., Aguayo, A., Bilbao, J., 2016b. Effect of the Acidity of HZSM-5 Zeolite and the Binder in the DME Transformation to Olefins. Ind. Eng. Chem. Res. 55, 1513-1521.

Plotkin, J.S., 2005. The changing dynamics of olefin supply/demand. Catal. Today 106, 10-14.

Raoof, F., Taghizadeh, M., Eliassi, A., Yaripour, F., 2008. Effects of temperature and feed composition on catalytic dehydration of methanol to dimethyl ether over γ-alumina. Fuel 87, 2967-2971.

Roberts, J.D., Caserio, M.D., 1977. Basic Principles of Organic Chemistry, 2nd ed. W. A. Benjamin, Inc., Menlo Park.

Rocha, T.C., Soares, B.G., Coutinho, F., 2007. The most important butadiene based elastomers employed in the automotive industry. Polimeros 17, 299-307.

Sardesai, A., 1997. Catalytic conversion of dimethyl ether to lower olefins: process and catalyst deactivation studies. Doctoral dissertation, University of Akron, Dept. of Chemical Engineering.

Sardesai, A., Lee, S., 2006. Alternative Source of Propylene. Energ. Source. 27, 489-500.

Stöcker, M., 1999. Methanol-to-hydrocarbons: catalytic materials and their behavior. Microporous Mesoporous Mater. 29, 3-48.

Valle, B., Castaño, P., Olazar, M., Bilbao, J., Gayubo, A.G., 2012. Deactivating species in the transformation of crude bio-oil with methanol into hydrocarbons on a HZSM-5 catalyst. J. Catal. 285, 304-314.

Zeng, C., Sun, J., Yang, G., Ooki, I., Hayashi, K., Yoneyama, Y., Taguchi, A., Abe, T., Tsubaki, N., 2013. Highly selective and multifunctional Cu/ZnO/Zeolite catalyst for one-step dimethyl ether synthesis: preparing catalyst by bimetallic physical sputtering. Fuel 112, 140-144.